Multidimensional Flux-Form Semi-Lagrangian Transport Schemes

SHIAN-JIANN LIN* AND RICHARD B. ROOD

Laboratory for Atmospheres, Goddard Space Flight Center, Greenbelt, Maryland

(Manuscript received 18 August 1995, in final form 22 February 1996)

ABSTRACT

An algorithm for extending one-dimensional, forward-in-time, upstream-biased, flux-form transport schemes (e.g., the van Leer scheme and the piecewise parabolic method) to multidimensions is proposed. A method is also proposed to extend the resulting Eulerian multidimensional flux-form scheme to arbitrarily long time steps. Because of similarities to the semi-Lagrangian approach of extending time steps, the scheme is called flux-form semi-Lagrangian (FFSL). The FFSL scheme can be easily and efficiently implemented on the sphere. Idealized tests as well as realistic three-dimensional global transport simulations using winds from data assimilation systems are demonstrated. Stability is analyzed with a von Neuman approach as well as empirically on the 2D Cartesian plane. The resulting algorithm is conservative and upstream biased. In addition, it contains monotonicity constraints and conserves tracer correlations, therefore representing the physical characteristics of constituent transport.

1. Introduction

Numerical modeling of advection is central to the approximate solution of fluid dynamical equations in many fields of science. Within atmospheric science, advection modeling is most closely associated with the solution of the equations of motion as well as the solution of the constituent continuity equation. As Kalman filter techniques are developed for model data assimilation, numerical advection algorithms will be required to accurately model the propagation of the statistical information that describes the error characteristics of the assimilation process (e.g., Cohn 1993).

As reviewed in Rood (1987), there have been many approaches to the solution of the advection equation in many fields of physics. These approaches have usually proceeded independently and many similar ideas have evolved. A common underlying problem is the fact that discrete numerical approaches inevitably introduce diffusion (or synonymically, dissipation) and dispersion into the approximate solution. The diffusion and dispersion errors can be viewed from either a mathematical or a physical point of view. From a physical point of view, advection of a passive tracer is the simple translation of a quantity. Therefore, dispersion, the propagation of different spatial scales at different phase speeds, and diffusion are processes that are alien to the process that is being modeled. As applied to the constituent advection problem, these numerical artifacts manifest themselves as nonphysical mixing by numerical diffusion, nonphysical highs and lows in the constituent field caused by dispersion, and nonphysical tracer spectra caused by the trapping of tracer in nonpropagating small spatial scales.

Just as the errors in the discretization of the advection equation can be viewed from either a physical or mathematical point of view, so can the derivation of algorithms to solve the advection equation. Mathematical approaches can be based on Taylor series expansions and the generation of discrete estimates of derivatives (e.g., Haltiner and Williams 1980). Within the field of gas dynamics, physical Eulerian approaches were pioneered by van Leer (1974) and Boris and Book (1973). These physical approaches are not content with simply assuring conservation. They also constrain the numerical solution to propagate information from upstream points (i.e., upstream-biased) and to create no new minima and maxima in the approximate solution. To counter the unavoidable diffusion and dispersion errors, maintenance of these physical constraints often required seemingly arbitrary engineering approaches of combining different solution methods when there was a danger of creating a nonphysical error.

In Rood (1987) it was argued and concluded that a straightforward approach, such as spatial fourth-order finite differences with leapfrog time differences, provided a cost-effective numerical algorithm. It was felt that many of the more sophisticated approaches pro-

* Current affiliation: General Sciences Corp., a subsidiary of Science Applications International Corp., Laurel, Maryland.

Corresponding author address: Dr. Shian-Jiann Lin, Data Assimilation Office, Laboratory for Atmospheres, NASA/Goddard Space Flight Center, Greenbelt, MD 20771.
E-mail: lin@dao.gsfc.nasa.gov

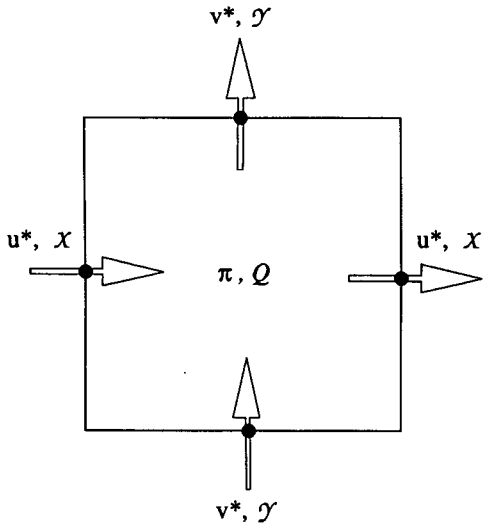

FIG. 1. Schematics of the C grid staggering of the time-averaged winds (u^*, v^*) and the density fields (π and Q). The fluxes $\mathcal{X}$ and $\mathcal{Y}$ are defined at the west (east) and south (north) interfaces of the cell, respectively.

vided only cosmetic improvement of the solution, but at significant expense. Real applications to atmospheric transport problems reveal that the conclusions of Rood (1987) were, at least, naive, if not wrong.

The Rood (1987) conclusions had been based on simulations of ozone and other tracers. Looking at both zonal-mean fields, as well as the evolution of tracers on latitude–longitude surfaces (e.g., Rood et al. 1991), the different schemes seemed to have little impact on the synoptic evolution. The rejection of the Rood (1987) conclusion comes from two sources. The first is the availability of very high quality aircraft tracer observations and the fact that compact correlations are observed between tracers. These correlations provide fundamental information about atmospheric transport and chemistry (Fahey et al. 1990; Plumb and Ko 1992), and a numerical model must be able to maintain correlation information if it is to be useful in quantitative studies. The second is the availability of winds from data assimilation procedures that allow direct, stringent comparisons between model simulations and observations (Rood et al. 1989). The use of assimilated data to perform transport experiments raises the level of comparison to a point where errors in the advection algorithm impact the ability to do science. The pursuit to improve atmospheric chemistry and transport modeling at NASA/Goddard Space Flight Center has led to the use and rejection of the square-root scheme (Schneider 1984), fourth-order finite differences with filling (see Rood 1987), and spectral methods using Forrester's filter (see Rood et al. 1991) because they did not credibly model the physics of advection and mixing. In addition, we have used the highly accurate scheme of Prather (1986), but its memory requirements for multiple tracer models have limited our applications.

Allen et al. (1991, A91 hereafter) provided a description of a simple and fast van Leer scheme applied to the atmospheric chemistry and transport problem. The diffusion and dispersion errors in this scheme manifest themselves as a significant spatially scale-dependent diffusion. The current paper describes an algorithm for creating multidimensional algorithms from the one-dimensional (1D) finite-volume schemes. These new algorithms have proven both more accurate and computationally faster than the A91 scheme, which has been used in several successful applications of the Goddard chemistry transport model (e.g., Douglass et al. 1993; Rood et al. 1993). Geophysical applications of the current scheme can be found in Douglass et al. (1996).

The development of the proposed algorithm will build on our generalization of 1D finite-volume schemes to multidimensions combined with an efficient algorithm to reduce the stringent time-step stability requirements, which is particularly important for the application in the spherical geometry. For the scheme to meet the physical constraints of tracer advection, we will require our algorithm to

1) conserve mass without a posteriori restoration,
2) compute fluxes based on the subgrid distribution in the upwind direction,
3) generate no new maxima or minima,
4) preserve tracer correlations,
5) be computationally efficient in spherical geometry.

In addition we will pay special attention to the problem of consistency between the tracer continuity equation and the underlying equation of continuity of the air. For example, chemistry transport models often use winds from a general circulation model or a meteorological model-assimilated dataset. This separation of the dynamical model and the off-line chemistry transport model could be viewed as process or time splitting in a generalized way (see McRae et al. 1982). When splitting techniques are used to solve a numerical problem as a series of successive partial steps, inconsistency often arises. This may be revealed by numerical instabilities that occur because, for instance, numerical terms in one equation are not properly balanced by terms in another equation. In the case of the chemistry transport model, the horizontal and vertical components of the winds satisfy the discrete form of the continuity equation in the wind-producing model. In general the winds will not be consistent with the discrete form of the tracer continuity equation. This inconsistency has been found to be deleterious, especially for long integrations or where direct, quantitative comparison with observations is required. In A91, the vertical velocity was recalculated using the tracer continuity equation. This yielded a scheme that would maintain a

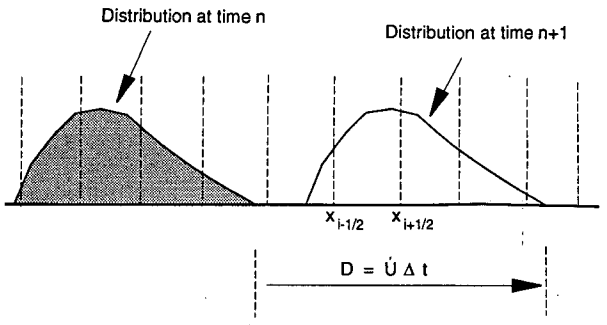

FIG. 2. Shape preserving translation of the distribution by the uniform flow U.

constant tracer as a constant without producing spurious fluxes or local conservation violations. However, the scheme also yielded nonphysical vertical velocity at the ground. While these did not impact the stratospheric ozone experiments, such an error in vertical velocity for tropospheric applications is unacceptable.

The algorithm for extending 1D schemes to multidimensions will be developed symbolically without specifying a particular 1D algorithm. This will allow flexibility to choose 1D schemes that provide the characteristics and accuracy needed for a particular problem. The 1D schemes chosen for implementation of the multidimensional algorithm will be 1D finite-volume schemes of the van Leer–type (van Leer 1974, 1977, 1979; Colella and Woodward 1984). The work follows directly from that of A91 and Lin et al. (1994, hereafter L94). To model the transport near poles more efficiently and accurately, we will seek an integration method analogous to the semi-Lagrangian approach that allows the use of time steps longer than those allowed in the explicit 1D Eulerian schemes. A disadvantage of the conventional semi-Lagrangian approach (see Staniforth and Côté 1991 for a review) is that mass conservation without a posteriori restoration or modification to the interpolation procedure is not assured (Priestley 1993). We will overcome this problem by formulating the semi-Lagrangian extension of the scheme in flux form, which ensures local and global mass conservation.

The algorithm to be developed in section 2 to extend the 1D finite-volume schemes to multidimensions has some features in common with other algorithms in the literature (e.g., Colella 1990; LeVeque 1993). We believe that the combination of physical attributes, flexibility, and computational efficiency is unique. The extension to long time steps is developed in section 3. The resulting algorithm is validated by a von Neumann stability analysis in appendices A and B and in a series of idealized experiments as well as in some geophysical applications in section 4. Concluding remarks are given in section 5.

2. Extension to multidimensions

In this section we present an algorithm to extend 1D forward-in-time advection schemes to multidimensions. This algorithm is independent of the particular numerics of the 1D scheme, but we will focus on finite-volume schemes of the van Leer–type (van Leer 1977, 1979; Colella and Woodward 1984; L94) in our applications. We shall restrict our attention to two space dimensions, x and y, which will be referred to as the east–west and north–south direction, respectively. Generalization to 3D is straightforward. The advective form of the conservation law for a conservative scalar is

$$\frac{\partial q}{\partial t} + \mathbf{V}\cdot\nabla q = 0, \tag{2.1}$$

where q represents a "mixing ratio–like" quantity, and $\mathbf{V} = (u, v)$ is the two-dimensional vector wind. The conservation law in flux form is

$$\frac{\partial \pi q}{\partial t} + \nabla\cdot(\pi q\mathbf{V}) = 0, \tag{2.2}$$

where π could be the density of a nonhydrostatic system, the surface pressure of a sigma-coordinate hydrostatic system, or the depth of the fluid of a shallow water system. The conservation law for π in flux form can be obtained by setting $q = 1$ in (2.2)

$$\frac{\partial \pi}{\partial t} + \nabla\cdot(\pi\mathbf{V}) = 0. \tag{2.3}$$

Note that the quantities that should be conserved are π and πq, not q. Numerical discretization of (2.1) will not, in general, conserve πq. On the other hand, conservation of πq is almost automatic if the flux-form conservation law (2.2) is discretized.

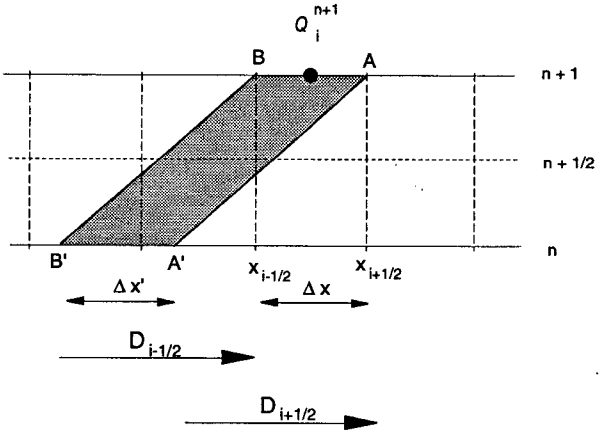

FIG. 3. The mass conservation law in the discretized 1D Lagrangian space. Winds defined at the mid–time level are used to compute the displacements ($D_{i-1/2}$) of the cell interfaces.

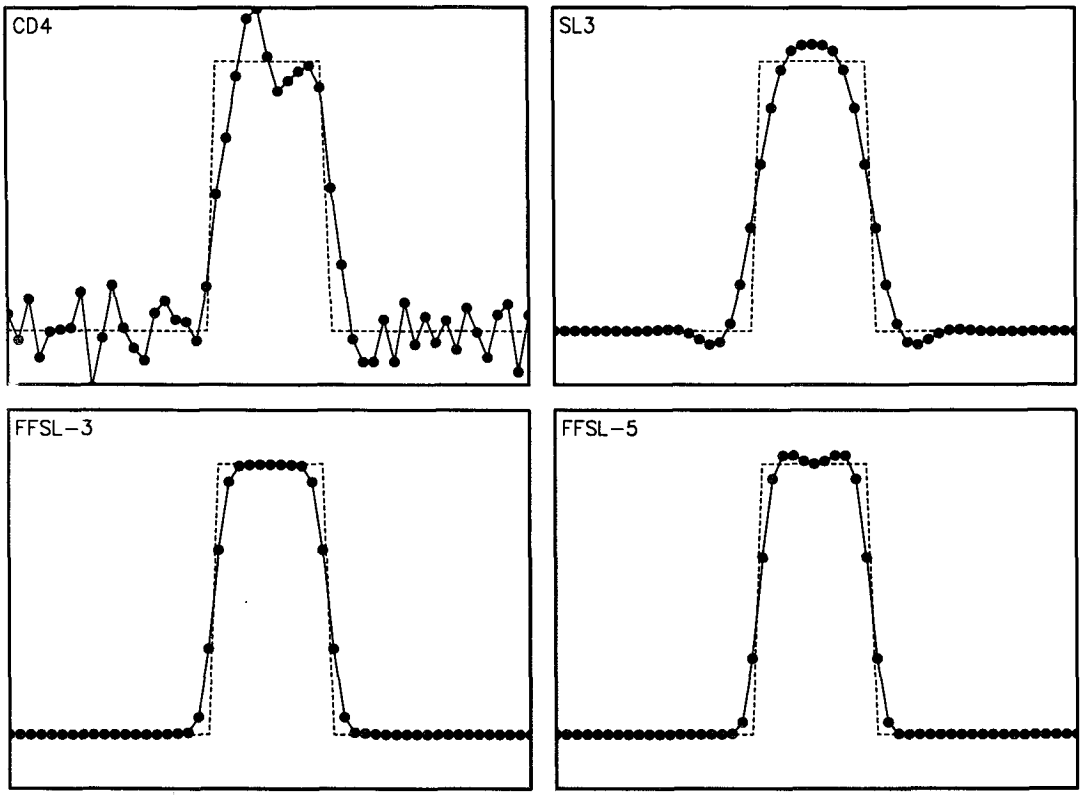

FIG. 4. The transport of a rectangular wave in a 50-cell periodic domain by (a) center differencing scheme (CD4, upper left panel), (b) semi-Lagrangian scheme based on the cubic interpolation (SL3, upper right panel), (c) modified monotonic PPM (FFSL-3, lower left panel), and (d) modified positive definite PPM (FFSL-5, lower right panel). Courant number is 0.5. Dashed line is the analytic solution.

Operator splitting is often used to extend 1D schemes to higher dimensions. Splitting is the process of replacing a complex problem by a series of more simple subproblems and often introduces errors, that can in the worse cases lead to the failure in multidimensional applications. In applications where the flow is nonhydrostatic and highly compressible, it has not been found necessary to eliminate the splitting error to have a successful simulation (e.g., Woodward and Colella 1984; Carpenter et al. 1990; Colella 1990). But for large-scale geophysical applications in which the flow is hydrostatic and nearly incompressible, modeling experience suggests that the splitting error must be explicitly considered. To extend 1D schemes to multidimensions, and to maintain the required attributes as defined in the introduction, the following are postulated as rules in the algorithm development:

(I) *Conservation:* The total constituent mass (global integral of πq) must be exactly conserved in the discretized form.

(II) *Consistency:* For a spatially uniform q field, the discretized form of (2.2) must degenerate to (i) the discretized form of (2.3) for a general flow field, or (ii) the discretized incompressibility condition $\nabla \cdot \mathbf{V} = 0$ when the flow is incompressible. Fulfillment of the this condition is *sufficient* to guarantee that a spatially uniform q field will remain uniform regardless of the compressibility (or divergence) of the flow.

(III) *Stability:* The CFL linear stability condition should be the same as for a directional split scheme; that is,

$$\max(C^x, C^y) \leqslant 1, \tag{2.4}$$

instead of the following more stringent condition

$$C^x + C^y \leqslant 1, \tag{2.5}$$

where $C^x = u\Delta t/\Delta x$ and $C^y = v\Delta t/\Delta y$ are the Courant numbers in the east–west and north–south directions, respectively. The stability condition (2.4) must be satisfied for the generalization to long time steps (see section 3) to work.

It is not a trivial matter to satisfy all three conditions simultaneously. An operator-split flux-form scheme can easily satisfy conditions I and III, but not II. An advective-form scheme will not, in general, satisfy condition I but will trivially meet condition II. The obvious consequence of violating condition II is that an initially

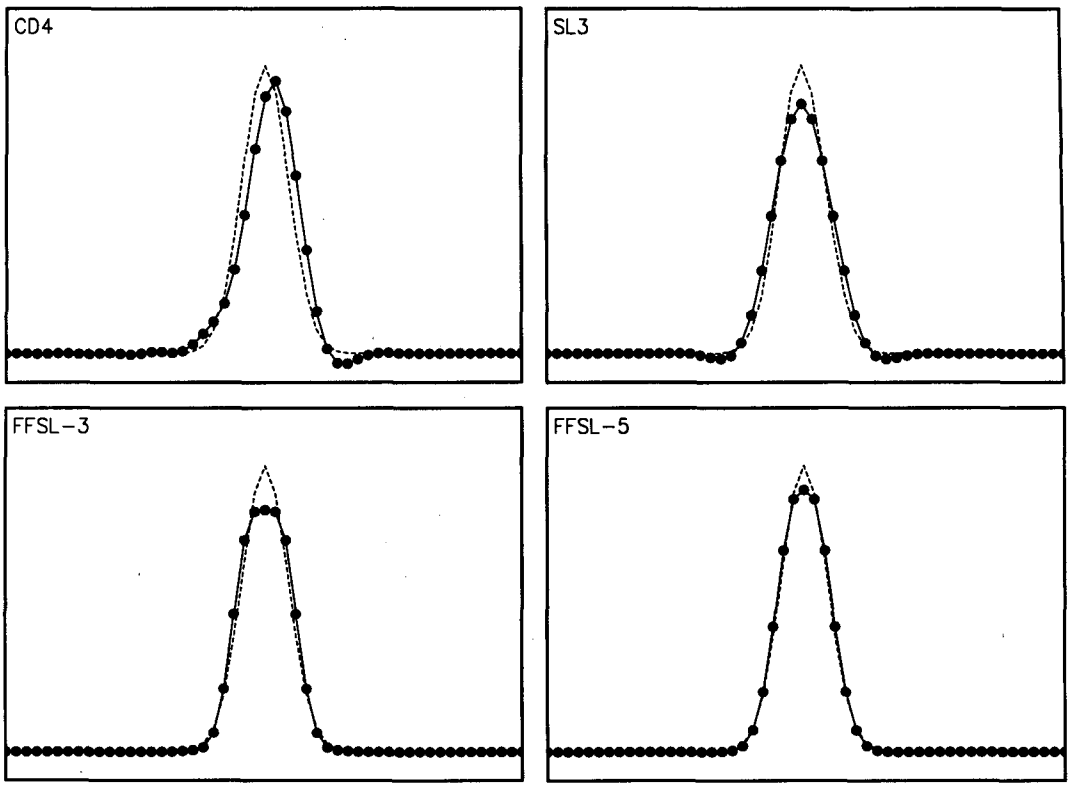

FIG. 5. As in Fig. 4 but for the Gaussian distribution.

constant mixing ratio field will not remain constant, and that adding a constant background value to a nonuniform distribution will affect the quality of the results. A less obvious and rarely discussed consequence of not satisfying II is that linear correlation between constituents will be lost even when the 1D scheme is perfectly linear (more discussions to be followed in this section and in section 4).

To develop the multidimensional algorithm without explicitly specifying the details of the 1D scheme, define F and G as the 1D operators representing "increments" (or updates) for one time step Δt to the constituent density field $Q\ (=\pi q)$ due to the flux-form transport from the east–west (x) direction and north–south (y) direction, respectively. Adopting the following standard difference notation δ,

$$\delta_\sigma S = S\left(\sigma + \frac{\Delta\sigma}{2}\right) - S\left(\sigma - \frac{\Delta\sigma}{2}\right), \quad (2.6)$$

F and G can be written as

$$F(u^*, \Delta t, \Delta x; Q^n) = -\delta_x[\mathcal{X}(u^*, \Delta t, \Delta x; Q^n)] \quad (2.7)$$

$$G(v^*, \Delta t, \Delta y; Q^n) = -\delta_y[\mathcal{Y}(v^*, \Delta t, \Delta y; Q^n)], \quad (2.8)$$

where $\mathcal{X}$ and $\mathcal{Y}$, the time-averaged fluxes of Q in the east–west and north–south direction, respectively, are defined as

$$\mathcal{X}(u^*, \Delta t, \Delta x; Q^n) = \frac{1}{\Delta x}\int_t^{t+\Delta t} uQdt - \text{HOT} \quad (2.9)$$

$$\mathcal{Y}(v^*, \Delta t, \Delta y; Q^n) = \frac{1}{\Delta y}\int_t^{t+\Delta t} vQdt - \text{HOT}, \quad (2.10)$$

where (u^*, v^*) are the time-averaged winds, and HOT represents the higher-order error terms. Other symbols and notations are standard. The very essence of 1D finite-volume schemes is to use a properly defined time-averaged (or time-centered) wind, u^* (or v^*), and the cell-averaged field at time-level n, Q^n, to approximate the "time-averaged" fluxes [the integrals in (2.9) and (2.10)] across the boundaries of the grid cell to predict the cell-averaged Q field at time level $(n + 1)$, Q^{n+1}. As illustrated in Fig. 1, the winds and the Q field are staggered as in the C grid (see Mesinger and Arakawa 1976 for the definition of grids A–E). For convenience, we will omit, in the rest of this section, the dependence of the F and G operators on (u^*, v^*), Δt, and Δx or Δy. For simplicity, we assume in the following analysis that the flow is nondivergent and π = constant (Q and q are therefore interchangable); that is, F and G are required to satisfy the following condition when $Q = \alpha$, an arbitrary constant.

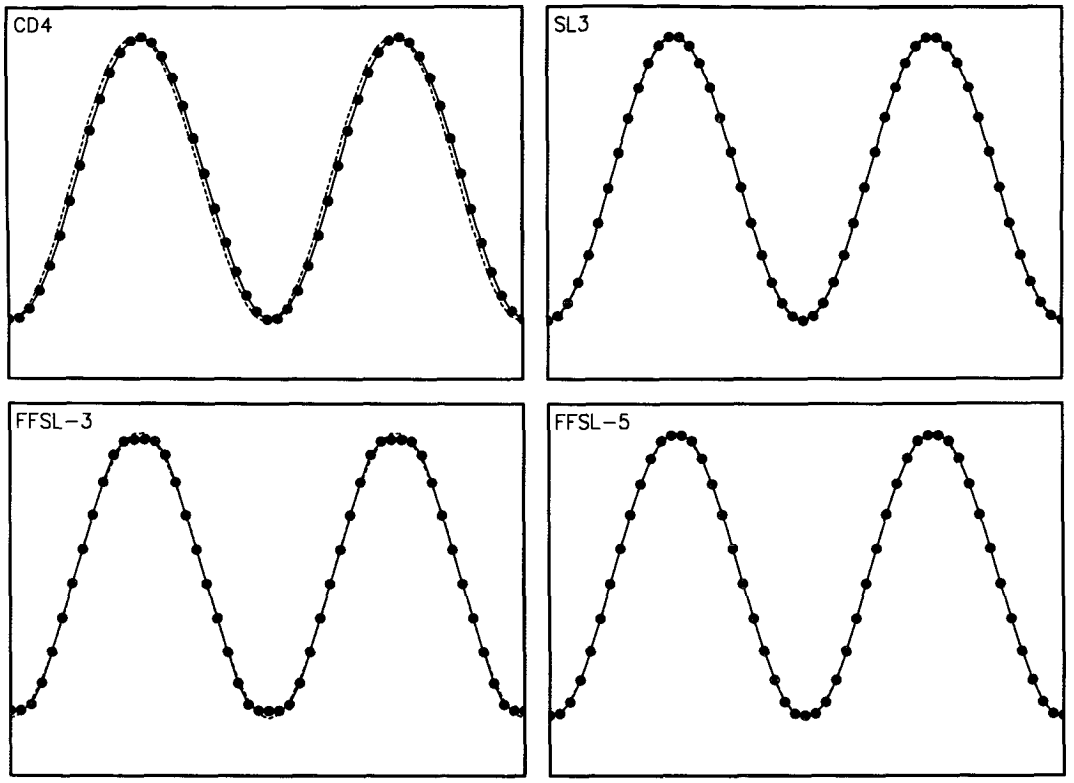

FIG. 6. As in Fig. 4 but for the wave-2 distribution.

$$F(\alpha) + G(\alpha) = -\alpha\Delta t\left(\frac{\delta_x u^*}{\Delta x} + \frac{\delta_y v^*}{\Delta y}\right) = 0. \quad (2.11)$$

Equation (2.11) is simply a 2D finite-difference representation of the divergence of the velocity field being equal to zero. In addition, F and G are required to satisfy the following relations

$$H(Q + \alpha) = H(Q) + H(\alpha) \quad (2.12)$$

$$H(\alpha Q) = \alpha H(Q), \quad (2.13)$$

where H represents a generic 1D flux-form increment operator (F or G). Equation (2.12) and (2.13) are the minimum conditions that must be met in order to preserve linear constituent correlations (see section 4c). Although the monotonic van Leer–type schemes as well as the piecewise parabolic method (PPM, Colella and Woodward 1984) are nonlinear, they all meet (2.11), (2.12), and (2.13). Positive definite schemes that correct only negative undershoots (e.g., the positive definite van Leer–type scheme in L94) are almost certainly to violate (2.12) and consequently will not, in general, preserve tracer correlations.

Using sequential splitting to advance the Q field one time step from time t^n to t^{n+1}, where $t^{n+1} = t^n + \Delta t$, first the F operator is applied in the x direction, followed by operating on the result of the x-advection with the y-advection operator G:

$$Q^x = Q^n + F(Q^n) \quad (2.14)$$

$$Q^{yx} = Q^x + G(Q^x). \quad (2.15)$$

Substituting (2.14) into (2.15) we obtain

$$Q^{yx} = Q^n + F(Q^n) + G(Q^n) + GF(Q^n), \quad (2.16)$$

where $GF(Q^n)$ is an abbreviation for $G[F(Q^n)]$. Here Q^{yx} is the predicted value at time $(n + 1)$. In deriving (2.16) we have assumed that G satisfies the following operation:

$$G[Q^n + F(Q^n)] = G(Q^n) + GF(Q^n), \quad (2.17)$$

which is exact unless a constraint of some sort (such as a positive definite or monotonicity constraint) is applied to render the operator G nonlinear. The consequences of this assumption will be addressed in section 4b.

The second and the third terms on the right-hand side (rhs) of (2.16) are the convergence of the orthogonal fluxes in the x and y direction, respectively, as if they were computed independently. The last term on the rhs of (2.16), which is introduced by the sequential splitting process, is critical to the stability of the scheme (Leith 1965; see also the stability analyses in appendix A). It has the appearance of a cross-derivative term and can be interpreted as the convergence of a secondary (oblique) flux that occurs because of the fact that the

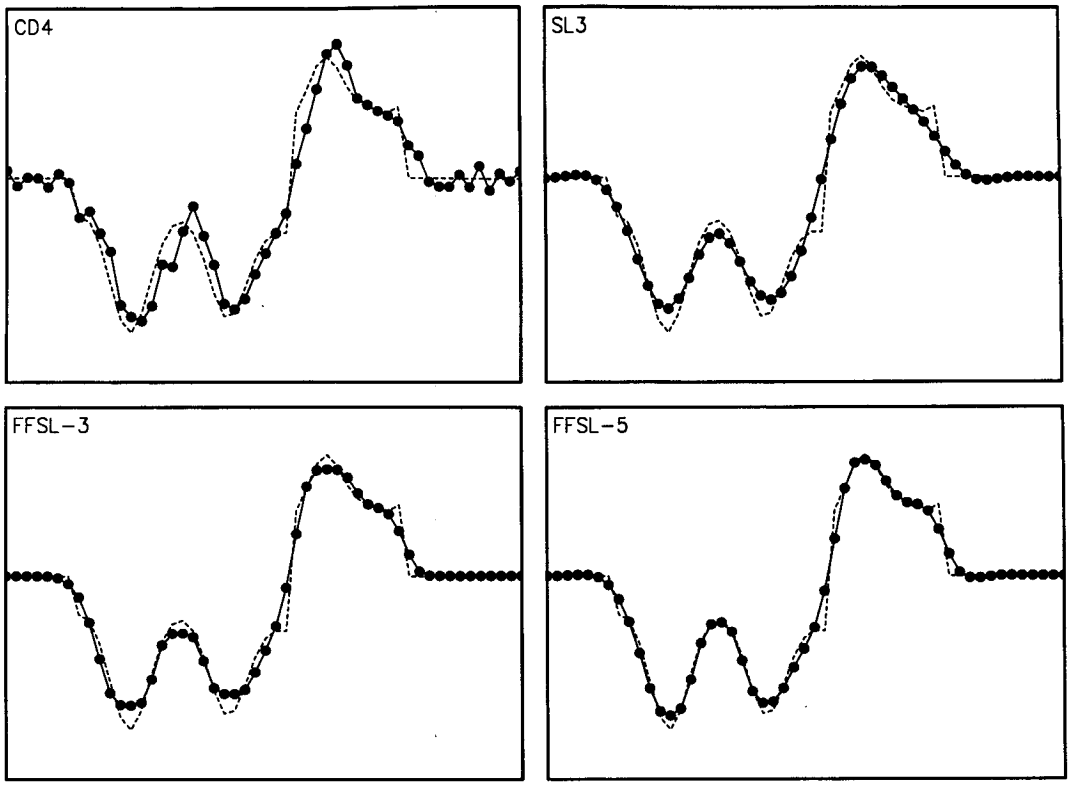

FIG. 7. As in Fig. 4 but for the irregular signal as in Smolarkiewicz and Grabowski (1990).

physical transport can neither be perfectly modeled by the independent applications of two orthogonal $F(Q)$ and $G(Q)$ operators nor can it be perfectly modeled by the sequential process (F followed by G) even when F and G taken individually are exact. This term will be identified as the splitting term, and it should vanish under the assumption that $\nabla \cdot \mathbf{V} = 0$ and $Q = \alpha$:

$$\alpha = \alpha + [F(\alpha) + G(\alpha)] + GF(\alpha). \quad (2.18)$$

Using (2.11), the two terms inside the square brackets vanish, and the error term, "$GF(\alpha)$," can be written as

$$GF(\alpha) = G\left(\frac{-\alpha\Delta t\delta_x u^*}{\Delta x}\right) \approx \frac{\alpha\Delta t^2\delta_y(v^*\delta_x u^*)}{\Delta x\Delta y}. \quad (2.19)$$

The above form is a center-differenced approximation because the exact form of the operator G has not yet been specified for a nonuniform Q field. It is clear that this term does not vanish for a deformational flow field (i.e., $\delta_x u^* \neq 0$).

If rather than performing the x advection followed by the y advection, the order were reversed, we obtain an equally valid scheme

$$Q^{xy} = Q^n + F(Q^n) + G(Q^n) + FG(Q^n), \quad (2.20)$$

and the splitting (error) term can be written as

$$FG(\alpha) = F\left(\frac{-\alpha\Delta t\delta_y v^*}{\Delta y}\right) \approx \frac{\alpha\Delta t^2\delta_x(u^*\delta_y v^*)}{\Delta x\Delta y}, \quad (2.21)$$

TABLE 1. Specifics of the multidimensional FFSL schemes on the sphere. Here C^x is the Courant number in the east–west direction. All inner operators are first-order accurate.

Scheme	Zonal operator (F) (when $C^x \leq 1$)	Zonal operator (F) (when $C^x > 1$)	Meridional operator (G) (Eulerian)
FFSL-1	first-order upwind	first-order upwind	first-order upwind
FFSL-2	monotonic van Leer	monotonic van Leer	monotonic van Leer
FFSL-3	monotonic PPM	monotonic van Leer	monotonic PPM
FFSL-4	semimonotonic PPM	monotonic van Leer	semimonotonic PPM
FFSL-5	positive-definite PPM	monotonic van Leer	positive-definite PPM

TABLE 2. Error statistics of six different transport schemes in the 1D 50-cell periodic domain for the rectangular wave after one revolution. Notations follow Rasch (1994).

Scheme	Courant number	Min	Max	L_1	L_2	L_∞
CD4	0.5	−0.2078	0.1961	0.4649	0.3116	0.5300
SL3	0.5	−0.0511	0.06273	0.2632	0.2583	0.3825
FFSL-2	0.5	0.	−0.0094	0.1818	0.2181	0.344
FFSL-3	0.5	0.	−0.0018	0.1439	0.1955	0.3181
FFSL-4	0.5	0.	0.0276	0.1525	0.1965	0.3549
FFSL-5	0.5	0.	0.03135	0.1459	0.1934	0.3462

which is antisymmetric (operator-wise) to (2.19). Both (2.16) and (2.20) are only first-order accurate due to the existence of the directional bias and the splitting error. Second-order accuracy can be obtained by a symmetric sequence of the operator splitting method (Strang 1968). A symmetric scheme can be readily obtained by averaging the two antisymmetric schemes (2.16) and (2.20); that is,

$$Q^* = \frac{1}{2}(Q^{xy} + Q^{yx}) = Q^n + F(Q^n) + G(Q^n) + \frac{1}{2}[GF(Q^n) + FG(Q^n)]. \quad (2.22)$$

Due to the elimination of the directional bias, (2.22) is expected to be more accurate than either (2.16) or (2.20), but it is also more expensive. [Given a fully second-order-accurate 1D scheme, second-order accuracy can be achieved by an alternating directional splitting procedure, but it does not eliminate entirely the directional bias.] To reduce total operation counts, (2.22) can be rewritten as

$$Q^* = Q^n + F\left[Q^n + \frac{1}{2}G(Q^n)\right] + G\left[Q^n + \frac{1}{2}F(Q^n)\right]. \quad (2.23)$$

Upon inspection, we see that all three schemes [Eq. (2.16), (2.20), and (2.23)] satisfy conditions I and III. (Stability of an asymmetric scheme is analyzed in appendix A). Condition II is more difficult to meet. Under the assumption that $\nabla \cdot \mathbf{V} = 0$ and $Q = \alpha$, there should be no change in Q^{xy}, Q^{yx}, or Q^* the predicted value at time $(n + 1)$. All three algorithms, however, predict a change proportional to the splitting term. To eliminate this error while satisfying conditions (I) and (III), we replace the inner operator F and G with their corresponding *advective* form operator f and g, respectively, to obtain

$$Q^{n+1} = Q^n + F\left[Q^n + \frac{1}{2}g(v_a^*, \Delta t; Q^n)\right] + G\left[Q^n + \frac{1}{2}f(u_a^*, \Delta t; Q^n)\right], \quad (2.24)$$

where

$$u_a^* = \overline{u^*}^x, \quad v_a^* = \overline{v^*}^y \quad (2.25)$$

are the winds at the cell center used by the inner advective operators. The overbars represent the following averaging operation (cf. 2.6):

$$\overline{S}^\sigma = \frac{1}{2}\left[S\left(\sigma + \frac{\Delta\sigma}{2}\right) + S\left(\sigma - \frac{\Delta\sigma}{2}\right)\right]. \quad (2.26)$$

Similar to their flux-form counterpart f and g, which also represent "increments" to the density field Q, approximate "$-\Delta t u_a^*(\partial Q/\partial x)$" and "$-\Delta t v_a^*(\partial Q/\partial y)$", respectively. Since outer operators are in the original flux form, condition I is still satisfied. The contributions from the advective form operators (the cross terms) vanish in the special case of a spatially uniform Q field. Condition II is thus satisfied. The advantage of maintaining the derivation in symbolic form allows the choice of building blocks (i.e., 1D inner and outer operators) that address conditions I–III, and hence, meeting the requirements outlined in the introduction.

TABLE 3. As in Table 2 but for the Gaussian distribution.

Scheme	Courant number	Min	Max	L_1	L_2	L_∞
CD4	0.5	−0.0352	0.0524	0.2735	0.2303	0.2089
SL3	0.5	−0.0185	−0.1342	0.1552	0.1291	0.1342
FFSL-2	0.5	0.	−0.1962	0.1628	0.1580	0.1962
FFSL-3	0.5	0.	−0.1532	0.1214	0.1183	0.1532
FFSL-4	0.5	0.	−0.0839	0.0563	0.0574	0.0839
FFSL-5	0.5	0.	−0.0839	0.0562	0.0574	0.0839

TABLE 4. As in Table 2 but for the wave-2 distribution.

Scheme	Courant number	Min	Max	L_1	L_2	L_∞
CD4	0.5	9.51E−3	−3.36E−3	6.30E−2	5.71E−2	4.96E−2
SL3	0.5	4.63E−3	−4.59E−3	5.90E−3	5.35E−3	4.65E−3
FFSL-2	0.5	3.56E−2	−3.20E−2	2.53E−2	2.68E−2	3.58E−2
FFSL-3	0.5	2.62E−2	−2.24E−2	1.81E−2	1.91E−2	2.63E−2
FFSL-4	0.5	2.62E−2	−7.54E−3	1.24E−2	1.42E−2	2.63E−2
FFSL-5	0.5	1.05E−2	−7.50E−3	5.76E−3	6.31E−3	1.06E−2

For the more general case that $\pi \neq$ constant, (2.24) can be modified and written in terms of the mixing ratio q

$$q^{n+1} = \frac{1}{\pi^{n+1}}\left\{\pi^n q^n + F\left[q^n + \frac{1}{2}g(q^n)\right] + G\left[q^n + \frac{1}{2}f(q^n)\right]\right\}. \quad (2.27)$$

Note that F and G have been redefined in (2.27) so that the operand is now q instead of Q (the π factor has been absorbed into the definition F and G by using properly defined mass fluxes in place of the velocities; see section 4c for the off-line transport case in which π is not a constant).

Since the cross terms are of higher order in time, it is sufficient to use the first-order upwind differencing for the two inner operators f and g to achieve an overall second-order accuracy. In the extension to long time steps (see next section) it will be necessary to use an unconditionally stable scheme for these two advective form operators. An example of constructing a second-order accurate 2D Eulerian scheme using (2.24) is given in appendix A where the stability of the scheme is analyzed. A more general example will be given in section 3.

Many methods have been developed in the past to reduce or eliminate the splitting error (e.g., Petschek and Libersky 1975; Dukowicz and Ramshaw 1979; Smolarkiewicz 1982 and 1984; Bell et al. 1988; Colella 1990; Ekebjærg and Justesen 1991; Bott 1993; LeVeque 1993). Although some of these methods are similar in spirit to the method just described, they are scheme specific. LeVeque (1993) derived a multidimensional scheme for the incompressible flow using the wave-propagation approach. If the van Leer schemes are chosen, our algorithm is then similar to LeVeque's method 4 (as described in his table labeled "algorithm 4.1"). There are two subtle differences. First, in computing the first-order upwind contribution from the transverse direction, velocities at cell edges are used in LeVeque's scheme instead of the cell-averaged velocities in our algorithm [see (2.25)]. Second, in (2.24) the contribution from the advective operator in the transverse direction will be added to Q^n and then subjected to the constraint associated with the 1D orthogonal flux operator (F or G), which is not the case in LeVeque's algorithm. For constant wind and if the unlimited van Leer scheme is chosen as the 1D flux-form operator, LeVeque's scheme and the scheme based on Eq. (2.24) (see appendix A) are in fact identical to the corner transport upwind algorithm developed by Colella (1990), which is derived from a very different perspective. The comparison with all other similar schemes as different choices are made for the 1D operators and velocity fields is beyond the scope of this paper. This paper proposed a general forward-in-time algorithm, defined symbolically by (2.24) or (2.27), with the flexibility to choose the advective and flux-form operators independently, and hence, to address the physical requirements of the advection problem.

3. Extension to large time steps

A disadvantage of explicit Eulerian schemes is that they have strict stability limitations, requiring the Courant number ($C^x = u\Delta t/\Delta x$) to be less than a specific scheme-dependent constant (usually $C^x \leq 1$). Since the stability requirement depends on the grid spacing, as higher-resolution grids are used the time step must

TABLE 5. As in Table 2 but for the irregular signal (Smolarkiewicz and Grabowski 1990).

Scheme	Courant number	Min	Max	L_1	L_2	L_∞
CD4	0.5	0.1307	0.1469	0.0861	0.1034	0.1726
SL3	0.5	0.2634	−0.1195	0.0623	0.0797	0.1755
FFSL-2	0.5	0.3582	−0.2139	0.0640	0.0847	0.1726
FFSL-3	0.5	0.2733	−0.1603	0.0480	0.0675	0.1452
FFSL-4	0.5	0.2680	−0.0576	0.0439	0.0654	0.1354
FFSL-5	0.5	0.1569	−0.0574	0.0344	0.0557	0.1327

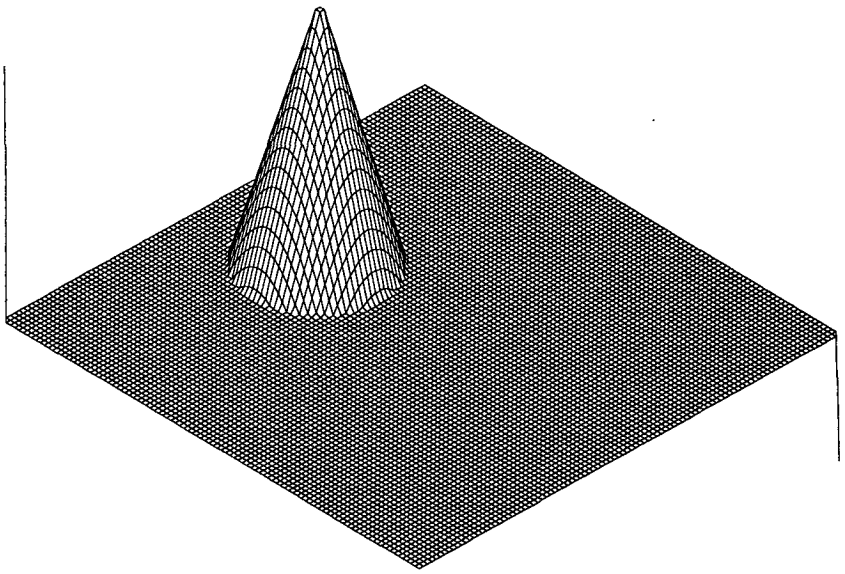

FIG. 8. The initial cone-shape density distribution.

also be reduced. Similarly, on equal angle spherical grids the convergence of meridians at the pole increases the cost of the scheme tremendously. Therefore, if a technique can be developed such that the stability is grid independent, then the time step can be chosen based on the physics and chemistry of the problem. This can yield a substantial economic savings which has been a major motivation for the development of semi-Lagrangian techniques for numerical weather prediction models (e.g., Bates and McDonald 1982; Williamson and Rasch 1989; Staniforth and Côté 1991). While the development presented below has some differences from the traditional semi-Lagrangian approach, the scheme does retain a Lagrangian (trajectory) character that is independent of time step. Thus, in the sense of meteorological terminology, the scheme is termed "flux-form semi-Lagrangian" (FFSL).

The extension to large time steps presented here is similar to approaches used by LeVeque (1985), Roache (1992), and Leonard (1994) for 1D Eulerian flux-form schemes. These authors do not present a generalization to multidimensions. Rancic (1992) devel-

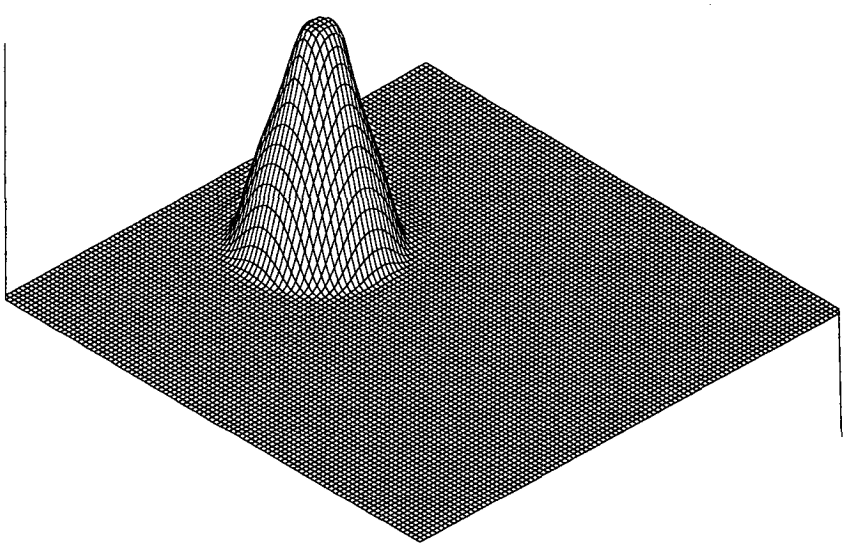

FIG. 9. The solution after 1508 time steps (the maximum Courant number is 2.5) using the PPM-based 2D FFSL scheme.

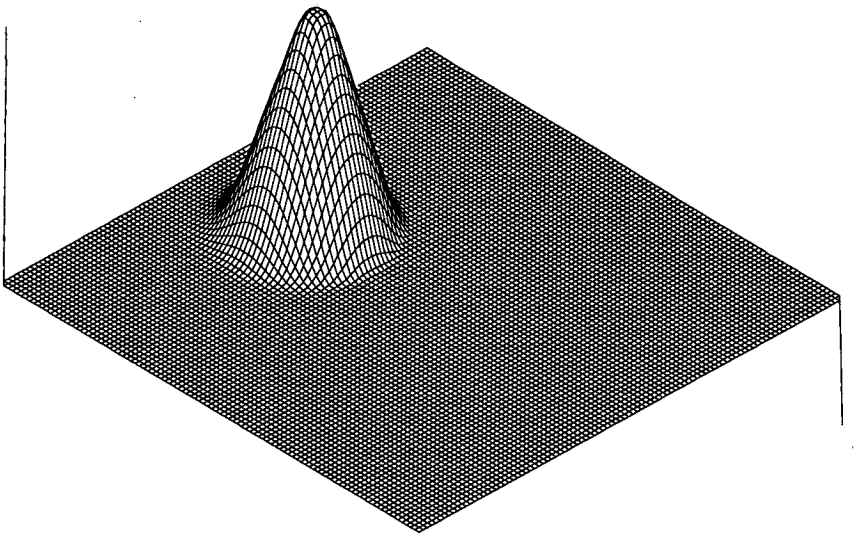

FIG. 10. The solution after 377 time steps (the maximum Courant number is 10) using the PPM-based 2D FFSL scheme.

oped a 2D semi-Lagrangian extension of the PPM based on a conservative remapping algorithm. As discussed in Laprise and Plante (1995), the 2D remapping algorithm does not, in general, preserve a constant tracer distribution due to the convergence/divergence induced by the cell deformation. This problem seems to be analogous to the error induced by operator splitting and does not appear to be important in compressible fluid models as suggested by the bubble convection test case in Laprise and Plante (1995). The FFSL scheme described here also bears some conceptual similarity to the "noninterpolating semi-Lagrangian scheme" (Ritchie 1986) and the semi-Lagrangian scheme of Smolarkiewicz and Pudykiewicz (1992). However, their methods are based on the advective form of the continuous equation, which does not guarantee mass conservation. Other novel approaches to increase the time step include the work of Brenier (1984) and Smolarkiewicz and Rasch (1991).

Consider the 1D advection problem with constant velocity as shown in Fig. 2. Assume that the tracer distribution is known continuously, and that the 1D space has been divided into uniformly spaced grid cells of width Δx. The velocity moves the field from left to right, and the advective process should simply translate the distribution while perserving its shape. The amount of material that is in the grid box bounded by $x_{i-1/2}$ and $x_{i+1/2}$ is updated by difference of flux into and out of the box [as in Eq. (2.7) or (2.8)]. For the constant velocity case the tracer distribution is simply translated by the distance $u\Delta t = D$, and the spatial translation is the same for both grid points $x_{i-1/2}$ and $x_{i+1/2}$. Here D is not limited for any physical reason to be less than Δx.

In the case that $u\Delta t = K\Delta x$, where K is an integer, then the advection is simply the translation of the entire distribution K grid boxes to the right, which can be treated exactly by many Eulerian transport schemes (see Rood 1987). Therefore, a strategy for extending schemes to long time steps is to use an integer translation for K grid boxes followed by a fractional translation, $c = \mathrm{mod}(C^x, K)$ (i.e., a shift operation, followed by an Eulerian advection calculation).

To develop the particular characteristics of the algorithm consider Fig. 3. On the abscissa is the spatial dimension x, divided into equal intervals of Δx. On the ordinate is time at steps n, $n + 1/2$, and $n + 1$ ($n + 1/2$ is not an actual step). We want to calculate the averaged density distribution at time $n + 1$ between grid points $x_{i-1/2}$ and $x_{i+1/2}$ based only on the distribution at time n. The velocity is left to right, but it is no longer required to be constant in space or in time. The heavy line $A'A$ that ends at the point $(i + 1/2, n + 1)$ is the trajectory from the previous time n. A similar trajectory $B'B$ is shown for the point $(i - 1/2, n + 1)$. At time $n + 1$, where the solution is being sought, the distance between B and A is Δx. Since the velocity is not required to be constant, the width of the cell between the two trajectories at time n, the distance between B' and A', is not Δx and will be labeled $\Delta x'$. We will model the spatial displacement from point A' to A, as $D_{i+1/2}$ equal to the "average velocity" along the trajectory $u_{i+1/2}^{n+1/2}$ multiplied by the time increment Δt. A similar average velocity is used for the trajectory $B'B$. The exact form of the average velocity will be defined below.

The problem posed in Fig. 3 focuses on the question, what spatial increment upstream at time n contains the

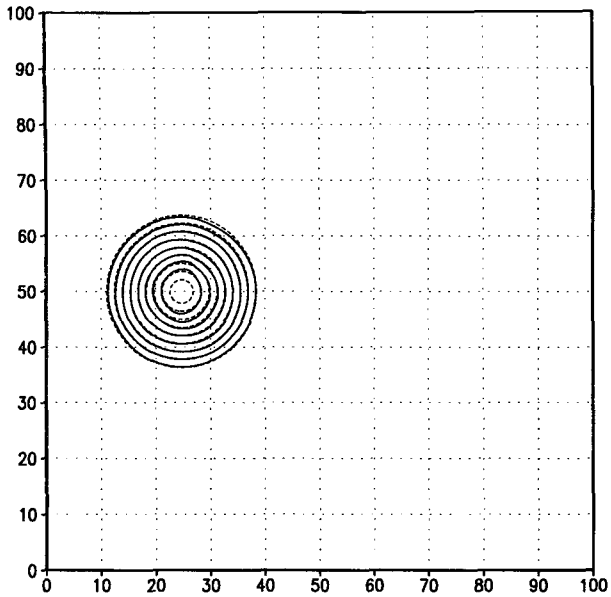

FIG. 11. As in Fig. 9 but the contour plot is shown. Initial distribution (dashed contours) is superimposed. Contour interval is 10% of the initial peak value. Zero contour is omitted.

mass that will be in the spatial cell of Δx size at time $n + 1$? Since, in the absence of sources and sinks, the mass is conserved between the trajectories (the shaded area in Fig. 3), if this question can be answered, mass will be conserved at time $n + 1$. Similarly, since the fluid is a continuous medium, as the same question is posed for all the grid points there will be a continuous mapping of the tracer at time n to time $n + 1$.

The problem in Fig. 3 should be contrasted with the usual semi-Lagrangian scheme that focuses on the grid point at i, $n + 1$ and asks the question, what point upstream arrives here? As is well known, the answer to this question does not a priori conserve mass. The problem in Fig. 3 can also be contrasted to normal Eulerian forward-in-time schemes, which approach the problem by mapping the field at time n (with the regular spatial interval Δx) to a generally irregular spacing $\Delta x'$ (due to flow deformation) at time $n + 1$, followed by an remapping back to the required regular interval.

For an arbitrarily long time step in the x direction the Courant number at point $i - 1/2$ can be written as

$$C^x_{i-1/2} = K_{i-1/2} + c_{i-1/2}, \tag{3.1}$$

where $K_{i-1/2}$ is the integer part of $C^x_{i-1/2}$, and $c_{i-1/2}$, the fractional Courant number, is given by

$$c_{i-1/2} = \mathrm{mod}(C^x_{i-1/2}, K_{i-1/2}). \tag{3.2}$$

The advection can then be broken down into an integer and fractional flux. Using the fractional Courant number $c_{i-1/2}$, the *fractional flux* can be computed by practically any Eulerian upstream flux-form scheme that utilizes the cell-averaged values to construct a subgrid distribution.

Denoting the cell-averaged density between $x_{i-1/2}$ and $x_{i+1/2}$ at future time $(n + 1)$ as Q^{n+1}_i, the 1D transport problem is

$$Q^{n+1}_i = Q^n_i + F_i = Q^n_i - (\delta_x \mathcal{X})_i. \tag{3.3}$$

Where F is now the "semi-Lagrangian" extension of the flux-form operator [see (2.7)] and $\mathcal{X}$, the "time-averaged" flux (see 2.9) at the left edge of the cell, is decomposed as

$$\mathcal{X}_{i-1/2} = (\text{integer flux})_{i-1/2} + (\text{fractional flux})_{i-1/2}. \tag{3.4}$$

The integer fluxes are computed exactly by

$$(\text{integer flux})_{i-1/2} = \begin{cases} \sum_{k=1}^{K_{i-1/2}} Q^n_{i-k}, & K_{i-1/2} \geqslant 1 \\ 0, & K_{i-1/2} = 0 \\ \sum_{k=1}^{-K_{i-1/2}} Q^n_{i-1+k}, & K_{i-1/2} \leqslant -1 \end{cases}. \tag{3.5}$$

To remain compliant with (2.11) [in order to meet condition II set forth in section 2], the "averaged velocity" along trajectory used to compute the displacement $D_{i-1/2} = u_{i-1/2}\Delta t$ of the cell interfaces is approx-

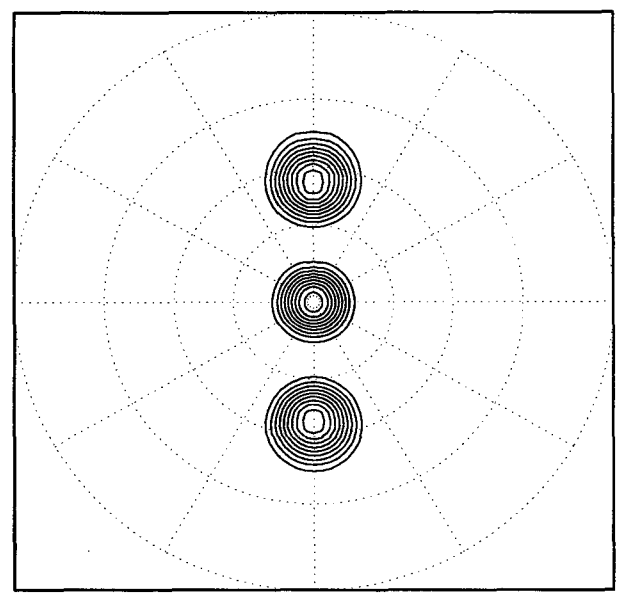

FIG. 12. Polar stereographic projection of the cosine bell (Rasch 1994) transported over the North Pole (from the bottom to the top of the figure) by the FFSL-5 scheme. Contour interval is 0.1 (zero contour is omitted). See Rasch (1994) for the analytic wind fields and initial condition.

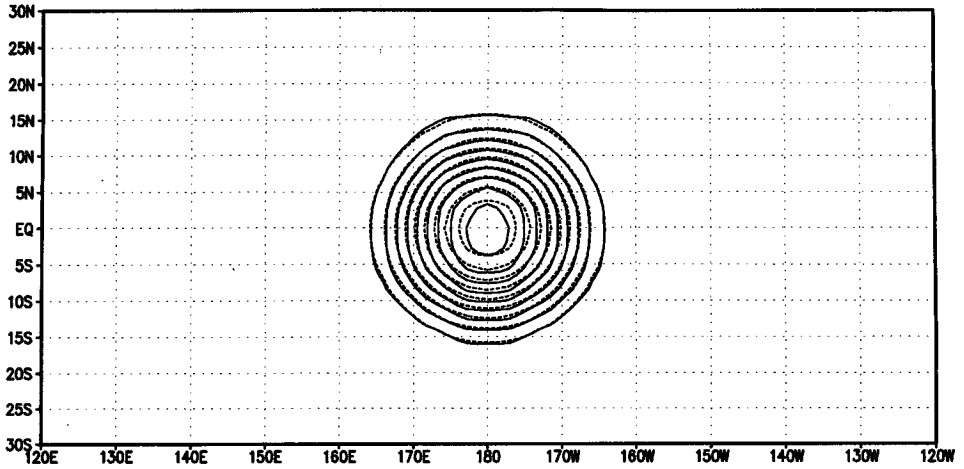

FIG. 13. Latitude–longitude projection of the cosine bell after one complete revolution by the FFSL-5 scheme. Exact solution (dashed contours) is superimposed. Contour interval is 0.1.

imated by the velocity given at $x = x_{i-1/2}$ and at time $(n + 1/2)$. Strictly speaking, the displacements (and hence the trajectories) of the cell interfaces computed this way are only first-order accurate. But they are used only in the computation of the fluxes, and their cell-centered differences [as computed in Eq. (3.3) for updating Q] are second-order accurate.

One criterion for the stability of the 1D scheme is that the trajectories of the left and right interfaces of a cell do not cross each other (i.e., the cell does not collapse during one time step) is simply

$$u_{i-1/2}^{n+1/2}\Delta t + \Delta x \geqslant u_{i+1/2}^{n+1/2}\Delta t$$

or

$$\frac{\Delta t \delta_x u^{n+1/2}}{\Delta x} \leqslant 1. \tag{3.6}$$

Equation (3.6) is, in fact, the condition that the deformational Courant number (or the Lipschitz number, see Smolarkiewicz and Pudykiewicz 1992) be less than unity. It can also be interpreted as the *smoothness* condition on the wind field u. This condition is much less restrictive than the normal Courant number limitation.

As in the restricted Courant number case described in section 2, the extension of the large Courant number case to 2D is achieved through the use of (2.24) or (2.27). The ability to make the long-time step extension to multidimensions relies on the flexibility of the scheme to use a different underlying 1D advection scheme for the inner operators, f and g [see (2.24)], than is used for the outer flux-form operator. To illustrate the development explicitly, specific inner (f and g) and outer operators (F and G) will be chosen. Stability requires that the 1D advective inner operator f (or g) be unconditionally stable for nondeformational flows. Practically any 1D version of the usual advective-form semi-Lagrangian scheme can be chosen. For efficiency, one should choose a low-order 1D advective-form semi-Lagrangian scheme (e.g., the first-order scheme based on the linear interpolation, see Bates and McDonald 1982). The advantage of using the first-order scheme for the inner operator is that it is both linear and monotonic, a unique combination. The trajectory calculation for the inner operator (f) uses the cell-averaged velocity as defined in (2.25)

$$u_a^{n+1/2} = \frac{1}{2}\left(u_{i-1/2}^{n+1/2} + u_{i+1/2}^{n+1/2}\right). \tag{3.7}$$

The 1D projection of the "departure point" x_*^n is then computed as

$$x_*^n = x_i^{n+1} - \Delta t u_a^{n+1/2}. \tag{3.8}$$

The values from two nearest grid cells to x_*^n at time n are then used in the linear interpolation procedure to obtain the advective update.

Following directly from (2.24) and (3.3) the 2D FFSL scheme (for an incompressible flow) in symbolic form is

$$Q^{n+1} = Q^n - \delta_x\left\{\mathcal{X}\left[Q^n + \frac{1}{2}g(Q^n)\right]\right\} - \delta_y\left\{\mathcal{Y}\left[Q^n + \frac{1}{2}f(Q^n)\right]\right\}. \tag{3.9}$$

We demonstrate here the construction of a 2D FFSL scheme using (3.9). Focusing only on the second term on the rhs of (3.9), to update Q_{ij}^n to Q_{ij}^{n+1}, the contribution from the first-order advective-form operator g at (i, j) can be written as

$$g_{ij} = (Q_{IJ}^n - Q_{ij}^n) + |c_{ij}^y|(Q_{IJ^*}^n - Q_{IJ}^n), \tag{3.10}$$

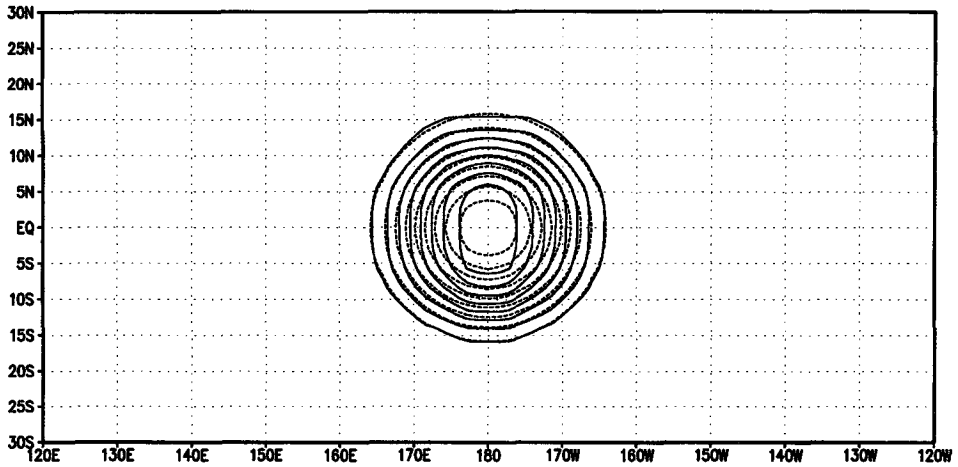

FIG. 14. As in Fig. 13 but for the FFSL-3 scheme.

where

$$C_{ij}^{y} = \frac{\Delta t}{2\Delta y}\,(v_{ij-1/2} + v_{ij+1/2}),$$

the Courant number at (i, j) in the y direction;

$c_{ij}^{y} = C_{ij}^{y} - \mathrm{INT}(C_{ij}^{y})$, the fractional Courant number at (i, j) in the y direction;

$$J = j - \mathrm{INT}(C_{ij}^{y}), \quad \text{and} \quad J^{*} = J - \mathrm{SIGN}(1, C_{ij}^{y}).$$

To complete the construction of the second term on the rhs of (3.9), we choose the second-order van Leer scheme as the outer flux-form operator. Defining Q_{ij}^{g} as the input tracer density field to $\mathcal{X}$; that is,

$$Q_{ij}^{g} = Q_{ij}^{n} + \frac{1}{2}\,g_{ij}(Q^{n})$$

$$= \frac{1}{2}\,[(Q_{IJ}^{n} + Q_{ij}^{n}) + |\,c_{ij}^{y}\,|(Q_{IJ^{*}}^{n} - Q_{IJ}^{n})], \quad (3.11)$$

the flux $\mathcal{X}$ across the left interface of the cell (i, j) is then computed as

$$\mathcal{X}_{i-1/2j} = (\text{integer flux})_{i-1/2j} + (\text{fractional flux})_{i-1/2j}, \quad (3.12)$$

where the fractional flux as computed by the van Leer scheme [cf. Eq. (1) in L94] is

$$(\text{fractional flux})_{i-1/2j} = c_{i-1/2j}^{x}\left\{ Q_{Ij}^{g} + \frac{\Delta Q_{Ij}^{g}}{2} \times [\mathrm{SIGN}(1, c_{i-1/2j}^{x}) - c_{i-1/2j}^{x}] \right\}, \quad (3.13)$$

where

$$C_{i-1/2j}^{x} = \frac{\Delta t u_{i-1/2j}}{\Delta x},$$

the Courant number at $\left(i - \frac{1}{2}, j\right)$,

$$I = \mathrm{INT}(i - C_{i-1/2j}^{x}), \quad M_{i-1/2j} = \mathrm{INT}(C_{i-1/2j}^{x}),$$

$$\Delta Q_{Ij}^{g} = \frac{1}{2}\,(Q_{I+1j}^{g} - Q_{I-1j}^{g}),$$

$$c_{i-1/2j}^{x} = C_{i-1/2j}^{x} - M_{i-1/2j},$$

the fractional Courant number at $\left(i - \frac{1}{2}, j\right)$.

A monotonicity constraint, if desired, can be applied to ΔQ_{Ij}^{g} using, for example, Eq. (5) in L94. Integer fluxes are computed by (3.5). The last term on the rhs of (3.9) can be similarly obtained. The above discretized form is written with its implementation on a vector processing computer in mind. Except for the computation of the integer fluxes, there will be no "IF" statement involved. The stability of the above scheme is analyzed in appendix B. It is shown that the scheme is unconditionally stable for nondeformational flows. The size of the time step will be limited by (3.6) for deformational flow. The above 2D scheme is second-order accurate. More accurate results can be achieved by using, for example, PPM for computing the fractional fluxes (3.13).

4. Numerical examples

For the implementation of the symbolic algorithm (2.24) the 1D monotonic van Leer–type scheme and the modified PPM are chosen as the basic building blocks of the multidimensional FFSL transport scheme. It is assumed that readers are familiar with both

TABLE 6. Error statistics for the "cosine bell test" (Rasch 1994) for Rasch's schemes and the FFSL schemes. Timings for the FFSL schemes are performed on the CRAY C-90. Meridional Courant number is 0.5. See Rasch (1994) for the definition of the error measures.

Scheme	Resolution	Time steps	Min	Max	L_1	L_2	L_∞	CPU (s)
FG2.8	128 × 64	256	−0.0411	−0.152	0.327	0.209	0.169	N/A
RG2.8	128 × 64	256	−0.0271	−0.150	0.289	0.176	0.164	N/A
RG2.8M	128 × 64	256	0	−0.210	0.181	0.158	0.196	N/A
RG1.4	256 × 128	512	−1.36E−2	−0.026	0.0647	0.0395	0.032	N/A
FFSL-1	128 × 64	256	0	−0.770	1.255	0.772	0.770	0.56
FFSL-2	128 × 64	256	−2.035E−4	−0.174	0.126	0.117	0.174	0.72
FFSL-3	128 × 64	256	−9.385E−4	−0.124	0.078	0.079	0.124	1.22
FFSL-4	128 × 64	256	−1.204E−3	−0.053	0.048	0.041	0.053	1.15
FFSL-5	128 × 64	256	−1.300E−3	−0.053	0.047	0.041	0.053	1.23
FFSL-3	256 × 128	512	−5.82E−4	0.040	0.020	0.020	0.040	9.8

schemes (see Carpenter et al. 1990 for a brief review of the PPM). In L94, the reference *mismatch* (or *slope* as conventionally defined) for the van Leer scheme is computed by a second-order difference of the cell-mean density [see Eq. (2) in L94 and (3.13) in the previous section]. It is verified numerically that sharper gradients can be maintained if the second-order mismatch is replaced by the following fourth-order difference one (see also Colella and Glaz 1985)

$$\Delta Q = \frac{1}{12}(8\delta_{2x}Q - \delta_{4x}Q). \tag{4.1}$$

The mismatch can then be monotonized with constraint (5) in L94. It is verified that PPM using this monotonized fourth-order mismatch instead of the original second-order one [Eq. (1.7) in Colella and Woodward 1984] gives better overall accuracy. Before applying the modified van Leer scheme and the modified PPM to multidimensions, it is informative to evaluate them in a simple 1D setting. Carpenter et al. (1990) has compared various schemes including a basic van Leer scheme, Smolarkiewicz's positive definite scheme (Smolarkiewicz 1983), and the original PPM in both 1D and 2D (using operator splitting). Although the van Leer scheme and PPM appear to perform very well in general, there is significant "clipping" of the peaks due to the strict monotonicity constraint (see their Figs. 6–9). To lessen this clipping effect, we propose the following two alternative constraints to be used by the PPM (alternative constraints for the van Leer–type schemes are given in L94): 1) the *semimonotonic* constraint, and 2) the *positive definite* constraint. The full monotonicity constraint as described in Colella and Woodward (1984) eliminates both undershoots and overshoots. The semimonotonic constraint eliminates undershoots but not overshoots, and the positive definite constraint prevents only the generation of negative values (see appendix C for details).

a. 1D comparisons

Figures 4–7 examine some standard 1D, 50-cell, periodic domain advection problems with constant wind. These problems clearly illustrate diffusion and dispersion errors. We will compare two FFSL schemes, one using the modified monotonic PPM (FFSL-3, hereafter) and the other using positive definite PPM (FFSL-5, hereafter) with the fourth-order center differencing scheme (CD4 hereafter) and a standard nonconservative semi-Lagrangian advection scheme based on the cubic interpolation (e.g., Bates and McDonald 1982, SL3 hereafter). Four distinctly different initial conditions are chosen. All schemes except CD4 are stable for arbitrary Courant number C. Since CD4 is unstable for $C > 0.73$, comparisons will be made at $C = 0.5$, which gives the most damped results for the van Leer–type scheme as analyzed in appendix A. Figure 4 shows the results after one revolution (100 time steps) for a rectangular wave. Figures 5, 6, and 7 show the results after one revolution for a Gaussian distribution, a wave-2 distribution, and an irregular signal (same as in Smolarkiewicz and Grabowski 1990), respectively. Visually, SL3 is the most diffusive, and CD4 is the most dispersive.

Error measures computed the same way as in Rasch (1994) following Williamson et al. (1992) are given in Tables 2–5. CD4 has the largest errors by nearly all measures. Also tabulated are results for the monotonic van Leer scheme (FFSL-2, hereafter) and the semimonotonic PPM (FFSL-4, hereafter). The accuracy of the second-order FFSL-2 scheme is comparable to SL3, and is significantly better than CD4 (for all tests). PPM-based schemes (FFSL-3, FFSL-4, and FFSL-5) are more accurate than SL3 except for the wave-2 test in which SL3 is marginally better than all FFSL schemes. All FFSL schemes maintain positivity of the original distribution and conserve mass exactly. Both semimonotonic and positive definite PPM maintain peaks better than the fully monotonic PPM, but at the risk of producing overshoots (see, e.g., Fig. 4).

b. 2D transport experiments

We will first demonstrate the stability and accuracy of the 2D FFSL scheme on the x–y plane with large Courant numbers. We will then turn our focus to the

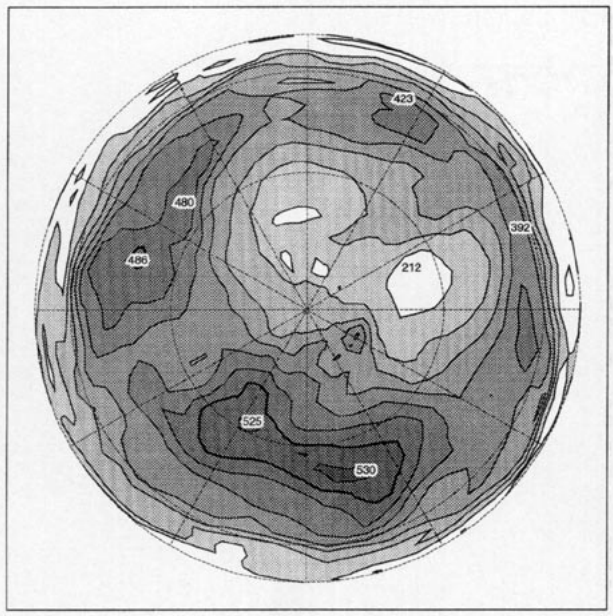

FIG. 15. Orthographic projection (0°–90°N) of the simulated total ozone (in Dobson units) at 1200 UTC 31 January 1989. Local maximum and minimum are printed. Contour interval is 40 (DU) and the bold contour is 480 (DU). The clear area is the "minihole."

implementation strategy on the sphere using a regular latitude–longitude grid.

The rotating cone experiment widely used in the literature (e.g., Smolarkiewicz 1983, 1984; Prather 1986; Smolarkiewicz and Grabowski 1990; Smolarkiewicz and Grell 1992) will be performed here to demonstrate the scheme on the 2D x–y plane. The initial condition (see Fig. 8) is a cone with unit height. The boundary condition for the advective field is doubly periodic, and there are 100×100 cells in the physical domain. We will examine the results after six revolutions. The modified PPM with monotonicity constraint is used as the outer flux-form operator in both spatial directions. The 1D version of the second-order semi-Lagrangian scheme (based on the quadratic interpolation; see, e.g., Bates and McDonald 1982) is chosen as the inner advective-form operator to match the higher-order accuracy of the PPM. All trajectory calculations are formally first-order accurate, as discussed previously. The resulting 2D scheme will not be strictly monotonic (i.e., over- and undershoots are possible) because only the 1D constraint is applied to the outer operator and there is no constraint of any sort applied to the inner second-order advective operator. Figures 9 and 10 show the results with maximum Courant number equal to 2.5 (1508 steps) and 10 (377 steps), respectively. [Courant numbers computed the same way as in Smolarkiewicz and Grell (1992).] Figure 11 shows the contour plot of the experiment with 1508 steps (as in Fig. 9). Mass is exactly conserved, and adding a large constant background value to the advected field does not change the final results. [The 2D scheme satisfies conditions (2.12) and (2.13)]. It is seen that the results are not overly sensitive to the size of the time step, and they compare very well against results in the literature when all factors (mass conservation, accuracy, speed, and memory requirement) are taken into consideration.

For the transport on the sphere, the so-called pole–Courant number problem is most severe in longitudinal (east–west) direction. To alleviate this problem and to maximize computational efficiency, we need only to apply the FFSL scheme in the east–west direction and use its faster purely Eulerian counterpart for the meridional (north–south) transport. Since the meridional transport is purely Eulerian, the same polar cap treatment in L94 can be used. The time step is therefore limited only by the meridional Courant number, that is, $C^y \leq 1$. To take advantage of the converging meridian at high latitudes, one can compute the *fractional fluxes* in the east–west direction using the faster but slightly more diffusive van Leer scheme if the *integer fluxes* [as defined by (3.5)] are nonzero (i.e., when $C^x > 1$) and use the less diffusive PPM-based schemes elsewhere. This time-saving modeling strategy also makes the effective zonal resolution more latitude independent. We have found this to be a very efficient combination that does not noticeably degrade the overall accuracy, as compared to the transport by PPM based schemes exclusively.

Rasch (1994) developed a 2D forward-in-time upwind-biased flux-form scheme that can be extended to the "reduced spherical grid" (RG). We repeat here his "cosine bell test" using various FFSL schemes (see Table 1 for specifics) on the regular (equi-angular) latitude–longitude grid. For the inner advective operator, all FFSL schemes use the 1D first-order semi-Lagrangian scheme described in section 3. The solid-body rotating cross-pole flow changes rapidly near the poles due to the use of the regular spherical grid. Operator-split flux-form schemes would exhibit some degree of deformational error. It is, thus, a very stringent test of the scheme's compliance to the three conditions set forth in section 2. For the sake of direct comparison, we used the same time step as Rasch (1994). Figure 12 shows the transport of the cosine bell structure using the FFSL-5 scheme (based on positive definite PPM) before, at, and after the North Pole. There is no deformational error as the structure approached and passed the pole, which is a significant improvement over the operator split version of the purely Eulerian van Leer scheme in A91 and L94 (see, e.g., Fig. 4 in A91). Figures 13 and 14 show the cosine bell after one revolution for the FFSL-5 and FFSL-3 schemes, respectively. Table 6 provides a detailed comparison between various FFSL schemes and Rasch's published results (copied from Rasch's Table 2). For convenience, pointwise values, instead of the cell-mean values, are used for the initialization and validation. The suffix M in RG2.8M indicates that a Zalesak-type (Zalesak

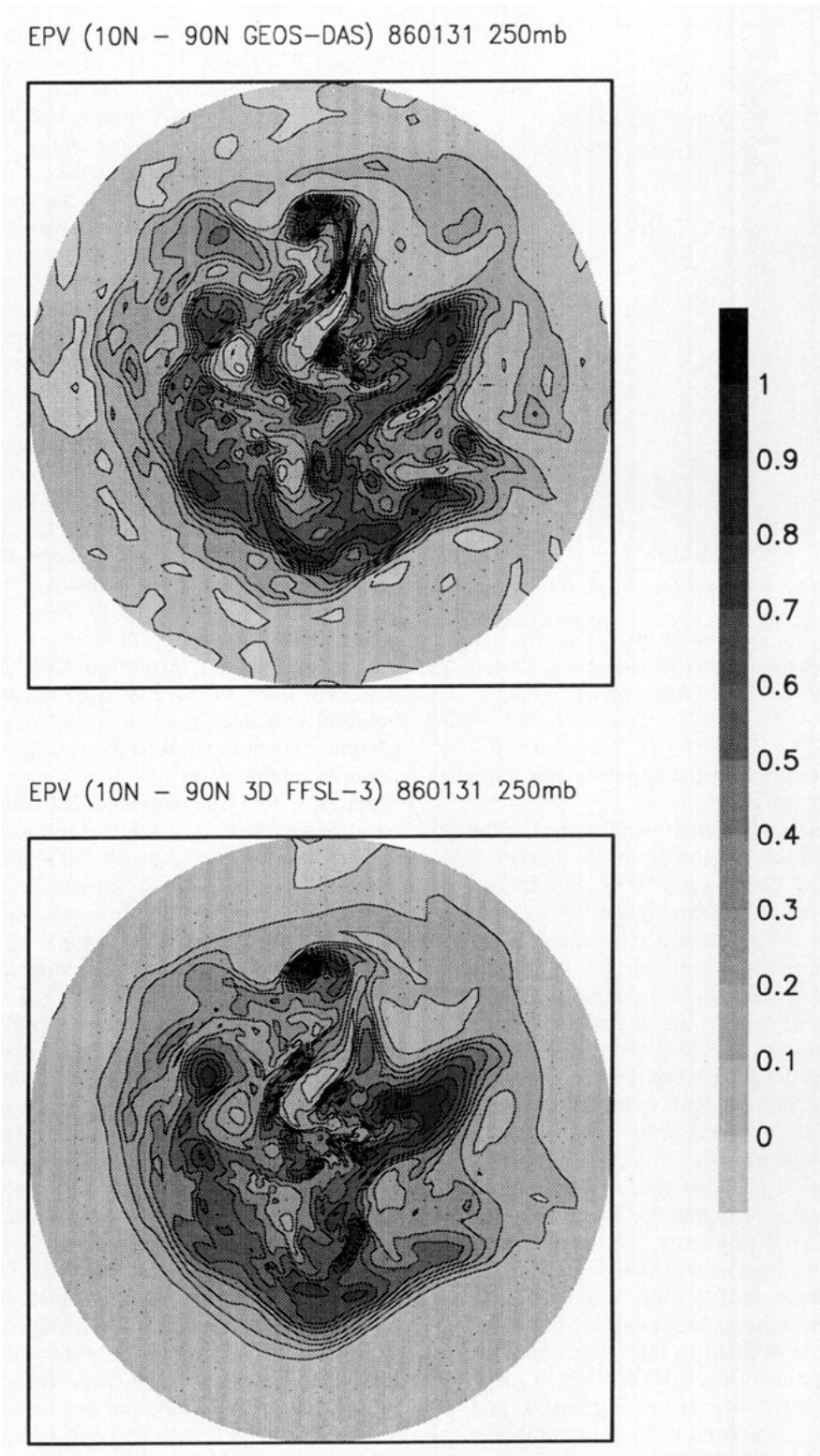

FIG. 16. Polar stereographic projection (10°–90°N) of the 250-mb Ertel potential vorticity (EPV) at 1200 UTC 31 January 1986. Upper panel: the "analysis" constructed directly from GEOS-DAS output. Lower panel: the simulation by the FFSL-3 scheme starting from 0000 UTC 1 January 1986.

1979) multidimensional monotonicity constraint has been applied to Rasch's schemes. It is seen that all FFSL schemes except the first-order upwind scheme-based FFSL-1 scheme are more accurate than Rasch's scheme, with or without constraint, on the reduced grid or the regular full grid (FG). The FFSL-3 and the FFSL-5 are roughly a factor of 2 and 4 more accurate than the RG2.8M, respectively. The FFSL-1 scheme is too diffusive to be useful. It is included in Table 6 for timing comparison. All FFSL schemes are vectorized on the CRAY C-90. It is seen that the FFSL-2 scheme is only 1.3 times slower than FFSL-1. PPM based FFSL-3, FFSL-4, and FFSL-5 schemes are about 2.2 times slower than the FFSL-1 scheme. It is seen that PPM-based schemes are considerably more accurate for a modest increase in CPU time.

The application of the 1D monotonicity constraint invalidated the assumption we made in the derivation of (2.24) or (2.27). The multidimensional FFSL schemes are, therefore, not strictly monotonic, even though the 1D operators are monotonic. We have found that if the cross-derivatives of the initial condition are continuous (smooth) then this is not a problem. For the cosine bell structure, which has discontinuities in the first derivative around its circular base, all the FFSL schemes except the first-order FFSL-1 produced some tiny negative values. Reducing the time step by 50% nearly reduced the negative undershoots to machine round-off. If a strict monotonic requirement becomes necessary, then a Zalesak-type multidimensional constraint to the FFSL schemes can be applied.

c. *Global 3D transport simulations*

In a global general circulation or chemistry transport models, the large-scale motions are quasi-horizontal and nearly incompressible. The vertical velocity, as diagnosed from the hydrostatic continuity equation, is more than an order of magnitude smaller than the horizontal velocity. The vertical transport can, therefore, be decoupled from the horizontal transport and computed *independently* (in the sense that the cross-derivative terms associated with the vertical advection are ignored). Denoting H as the 1D operator for the vertical transport (similar to F and G defined in section 2), the scheme for the 3D transport can be written as [cf. (2.27)]

$$q^{n+1} = \frac{1}{\pi^{n+1}}\left\{\pi^n q^n + F\left[q^n + \frac{1}{2}g(q^n)\right] + G\left[q^n + \frac{1}{2}f(q^n)\right] + H(q^n)\right\}. \quad (4.2)$$

It is understood that in computing the mass convergence terms (F and G) the time centered (or time averaged) winds (u^*, v^*) and surface pressure (π^*) defined at time ($n + 1/2$) are to be used. To verify "consistency" (condition II), the equation for π, the surface pressure, can be obtained by setting $q = 1$ in (4.2) and integrating from the top to the bottom of the vertical σ domain to obtain

$$\pi^{n+1} = \pi^n + \int_{\sigma_{\text{top}}}^{\sigma_{\text{bottom}}} [F(1) + G(1)]d\sigma \approx \pi^n - \Delta t \sum \left[\frac{\delta_x \overline{\pi^*}^x u^*}{\Delta x} + \frac{\delta_y \overline{\pi^*}^y v^*}{\Delta y}\right]\Delta\sigma_\kappa, \quad (4.3)$$

where $\Sigma\,[\ ]\Delta\sigma_\kappa$ represents the summation over the whole vertical (σ coordinate) domain. In reaching (4.3), a straightforward average of π to the cell interfaces is used to compute the horizontal mass fluxes ($\overline{\pi^*}^x u^*$, $\overline{\pi^*}^y v^*$). Equation (4.3) is simply a second-order center-differenced scheme for updating the surface pressure π on the C grid (see Fig. 1), which is the differencing scheme used in the Goddard Earth Observing System General Circulation Model and Data Assimilation System (GEOS-GCM and GEOS-DAS; see Schubert et al. 1993; Takacs et al. 1994). No special modification to the π equation is therefore needed to meet condition II.

Because of the quantitative use of tracer correlations (Fahey et al. 1990; Plumb and Ko 1992), a requirement of the scheme as outlined in the introduction is to conserve tracer correlations. We present here the proof that the 3D scheme (4.2) based on a 1D monotonic van Leer–type scheme, which is nonlinear, maintains exact linear constituent correlations in a pressure coordinate system (i.e., π = const) in which the mixing ratio and density fields of a constituent are equivalent. The

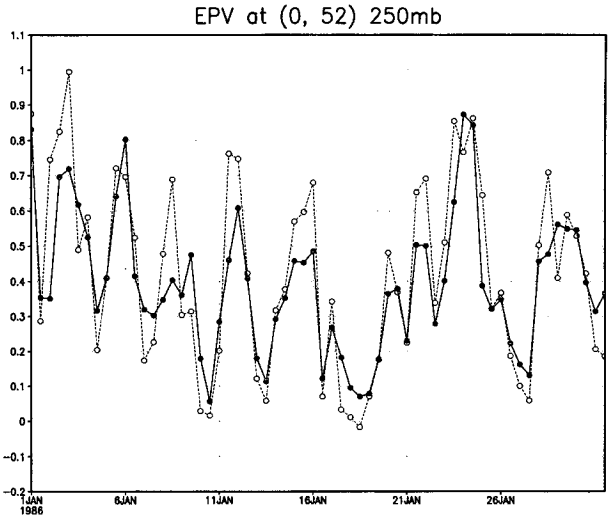

FIG. 17. Time series of the 250-mb EPV near London. Solid line: simulation. Dashed line: the "analysis." Values are plotted every 12 h.

equivalent condition to (2.11) in the 3D pressure-coordinate system is

$$F(\alpha) + G(\alpha) + H(\alpha) = 0. \quad (4.4)$$

Suppose the mixing ratios of two chemistry species p and q are linearly correlated at time n as

$$q^n = \alpha p^n + \beta, \quad (4.5)$$

where α and β are two arbitrary constants. We will show that after one time step the linear relationship between p and q is still preserved; that is, $q^{n+1} = \alpha p^{n+1} + \beta$. The transport scheme (4.2) for q in the pressure coordinate system is simply

$$q^{n+1} = q^n + F\left[q^n + \frac{1}{2}g(q^n)\right] + G\left[q^n + \frac{1}{2}f(q^n)\right] + H(q^n). \quad (4.6)$$

All monotonic van Leer–type 1D schemes discussed in L94 satisfy condition (2.12) and (2.13), which can be readily verified by inspecting (1a)–(1c), (2), and (5c) in L94. Substituting (4.5) into (4.6) and utilizing (2.12), (2.13), and (4.4), we have

$$q^{n+1} = \alpha\left\{p^n + F\left[p^n + \frac{1}{2}g(p^n)\right] + G\left[p^n + \frac{1}{2}f(p^n)\right] + H(p^n)\right\} + \beta = \alpha p^{n+1} + \beta.$$

We have built a global 3D chemistry transport model based on (4.2). We repeated the same ozone transport experiment in A91 using the FFSL-3 scheme (see Table 5) in the horizontal with 4° × 5° (latitude–longitude) resolution and semimonotonic PPM in the vertical direction. The time step is 30 min. No negative ozone mixing ratios are ever produced during the integration period (more than one month), and the results are comparable to A91's result using a basic Eulerian van Leer scheme with the higher 2° × 2.5° resolution (cf. Fig. 15 to Fig. 6 in A91). As a final demonstration of the accuracy and efficiency of the 3D FFSL schemes on the sphere, we consider the global transport of the Ertel potential vorticity (EPV) as a passive tracer. EPV, which has a very high vertical gradient, is chosen to test the effects of ignoring the cross terms associated with vertical advection. Winds and the surface pressure needed for the transport calculation are taken from the 5-yr reanalysis with the GEOS-DAS. Initial condition (at 0000 UTC 1 January 1986) for the transport is first constructed on pressure surfaces and linearly interpolated onto the transport model's σ surfaces. Figure 16 shows the "analyzed" 250-mb EPV field (upper panel) at 1200 UTC 31 January 1986 as constructed directly from the GEOS-DAS's output data and the corresponding simulation (lower panel) with the essentially monotonic FFSL-3 scheme (2° × 2.5° horizontal resolution with 20 vertical σ levels, 15-min time step). The simulation captures practically all large-scale features of the "analysis." Figure 17 shows the time series of the 250-mb EPV at the closest grid point to London (52°N, 0°). The correlation between the "analysis" and the simulation is very high, and it does not deteriorate with time. We did not use the less diffusive FFSL-4 (semimonotonic PPM) or the FFSL-5 (positive definite PPM) because EPV is not a positive definite scalar. The simulation took about 23 s CPU time (on a single processor CRAY C-90) per model day. We also experimented with an algorithm that included the cross terms in the vertical direction. It is found that the result is essentially identical to the one just presented without the associated vertical cross terms. This indicates that the simplification we took in deriving (4.2) is fundamentally sound under the hydrostatic assumption.

5. Concluding remarks

We have presented an algorithm for extending 1D flux-form transport schemes to multidimensions and large time steps. We have termed the scheme flux-form semi-Lagrangian (FFSL). The scheme is conservative and upstream-biased, and also has a monotonicity option. Two more subtle constraints are explicitly considered in the development. The "consistency" condition ensures that for constituent applications the numerical form of the constituent continuity equations becomes the same as the underlying continuity equation of the background fluid flow when the mixing ratio is constant. This seemingly trivial constraint is often not maintained in off-line tracer transport models and can cause spurious fluxes in the constituent field, which corrupts the ability to perform quantitative analysis. The second constraint is the ability of the nonlinear advection algorithm to preserve linear tracer correlations. High-quality tracer observations explicitly show compact correlation of transport dominated constituents (Fahey et al. 1990; Plumb and Ko 1992). Chemical sources and sinks can violate the correlation relationship. Hence, if a chemistry transport model is going to be used to study chemical mechanisms, the advection algorithm must be able to maintain the correlation relationship.

The multidimensional algorithm, which is derived from an operator-split perspective that explicitly considers the fluxes associated with the cross terms, allows the application of 1D monotonic van Leer–type schemes in multidimension. The splitting error in multidimensions is addressed by first symmetrizing the cross-derivative terms and then by enforcing an invariant condition of the advective form of the conservation law that a constant mixing ratio–like field should remain constant. The extension to long time steps can be

viewed as an integer shift of the distribution followed by a normal application of the Eulerian scheme. Due to the pole singularity, the multidimensional scheme would not be efficient in the spherical geometry without the semi-Lagrangian approach to eliminate the time step constraint. On the other hand, the full benefit of the conservative FFSL approach would not be realized without the multidimensional technique (the maximum allowable time step would be greatly reduced without the correct cross terms).

We have chosen the van Leer scheme and PPM as the building blocks of the multidimensional FFSL scheme due to their demonstrated accuracy and efficiency in 1D. PPM is a high-order extension of the van Leer scheme. It is often regarded as very expensive in the meteorology literature. Since a Riemann solver (see, e.g., Carpenter et al. 1990) is not involved for the constituent transport problem, our implementation of the 1D PPM (with first-order backward trajectory of the cell interface, see Fig. 3) to the multidimensional FFSL algorithm is computationally efficient, as demonstrated by the numerical example in sections 4b and 4c.

We recommend the use of the semimonotonic or the positive-definite constraint (for PPM) for low-resolution simulations or when there is explicit "subgrid-scale turbulence parameterization." For chemical constituents or water vapor transport in a general circulation model with moderate resolution, we recommend using the monotonic PPM in the horizontal and either semimonotonic or positive-definite PPM in the vertical direction. However, the monotonic constraint should always be used when preservation of the linear correlation is desired.

Our focus in this paper is on the tracer advection problem in the spherical geometry. A PPM-based multidimensional FFSL shallow-water model has been developed and presented in the fourth CHAMMP workshop for the numerical solution of PDE's in spherical geometry (Chicago, Illinois, 24–26 August 1994). A 3D plug-compatible "dynamical core" for the GEOS-GCM (Takacs et al. 1994) has also been developed and is currently under testing.

Acknowledgments. This work is supported by the NASA Atmospheric Effects of Aircraft Program and the algorithm has been provided to the Global Modeling Initiative at Lawrence Livermore National Laboratory. Computational support is provided through the Earth Observing System Program. We wish to thank Dr. P. Rasch and three anonymous reviewers for their comments, which have helped improve the manuscript. We also acknowledge Dr. B. Leonard for his comments on the manuscript. In addition, we want to thank Drs. S. Zalesak and A. Douglass for their reading of the manuscript and their support of the effort. We also thank Dr. P. Smolarkiewicz for his advice and editorial assistance.

APPENDIX A

Stability of the 2D Eulerian Flux-Form Schemes

The stability of the multidimensional flux-form scheme (2.24) can be analyzed by a von Neumann-type Fourier analysis (e.g., Haltiner and Williams 1980). It is not feasible to carry out such an analysis with a nonlinear scheme. We will choose the second-order van Leer scheme without a limiter as the 1D flux-form outer operator F (and G) and the first-order upwind scheme (the donor-cell scheme) as the 1D advective-form inner operator g (and f). It is convenient in the analysis to assume that U, V, and π are positive constants. Under such an assumption, the flow is nondeformational and nondivergent. Here Q (density) and q (mixing ratio) are, therefore, interchangeable. For a constant Courant number ($C^x = U\Delta t/\Delta x$), the unconstrained (i.e., linear) van Leer scheme in the x direction can be written in the following finite-difference form

$$q_{ij}^{n+1} = q_{ij}^n + F_{ij}(q^n), \tag{A.1}$$

where

$$F_{ij}(q^n) = C^x\Big[(q_{i-1j}^n - q_{ij}^n) - \frac{1}{4}(1 - C^x) \times (q_{i+1j}^n - q_{ij}^n - q_{i-1j}^n + q_{i-2j}^n)\Big]. \tag{A.2}$$

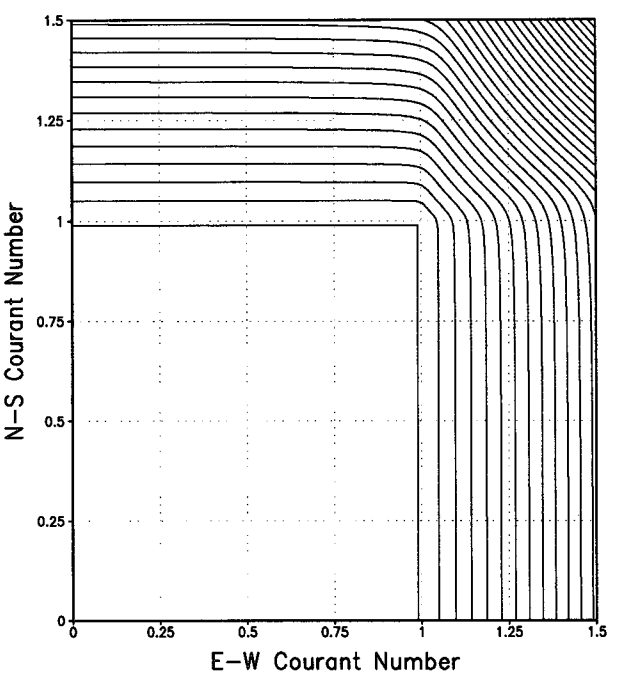

FIG. A1. The maximum amplification factor for the 2D Eulerian scheme (with linear second-order van Leer scheme as 1D outer operators). Contour interval is 0.1. The first contour is 1.

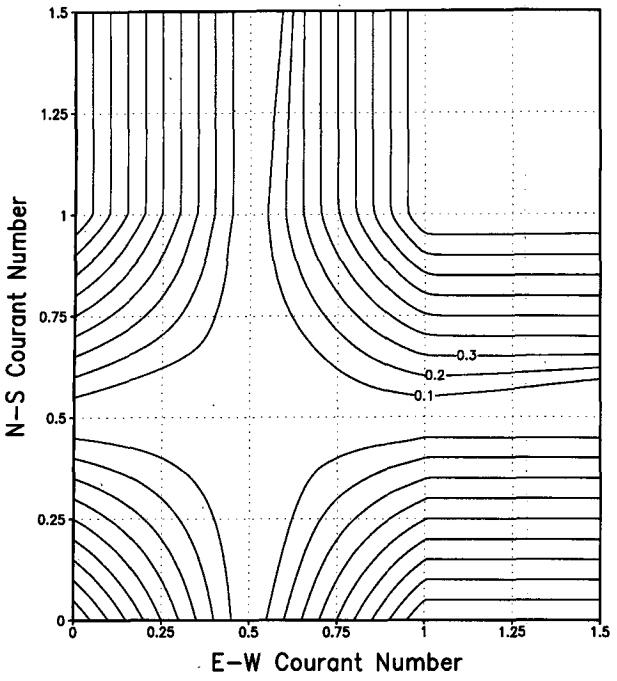

FIG. A2. As in Fig. A1 but for the minimum amplification factor. Contour interval is 0.1.

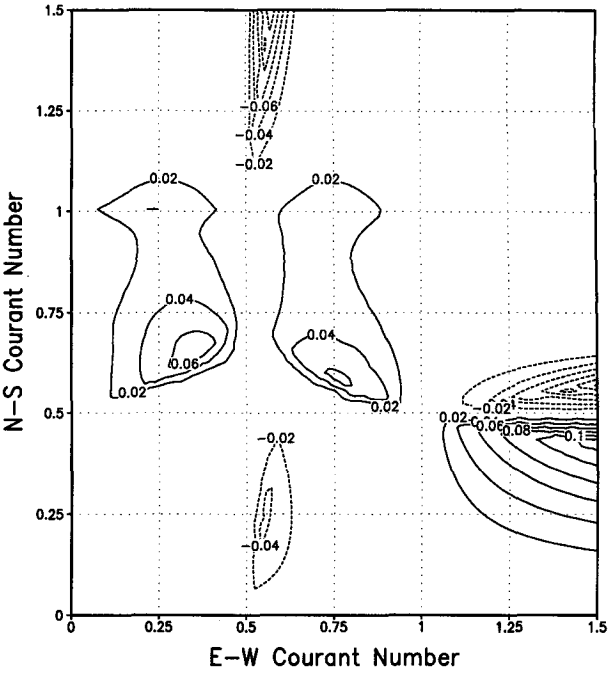

FIG. A3. The minimum amplification factor of the symmetric scheme (2.24) minus that of the asymmetric scheme (2.16).

The first-order upwind scheme (the donor-cell scheme) for the advective operator in the y direction is simply

$$q_{ij}^{n+1} = q_{ij}^{n} + g_{ij}(q^n), \tag{A.3}$$

where

$$g_{ij}(q^n) = C^y(q_{ij-1}^{n} - q_{ij}^{n}). \tag{A.4}$$

The second term on the right-hand side of (2.24) is obtained by replacing q^n in (A.2) with q^g, where

$$q^g = q_{ij}^{n} + \frac{1}{2} g_{ij}(q^n)$$

$$= q_{ij}^{n} + \frac{1}{2} C^y(q_{ij-1}^{n} - q_{ij}^{n}). \tag{A.5}$$

The remaining (last) term on the right-hand side of (2.24) can be easily obtained by the symmetric property of the scheme. Under the above assumption of constant winds, it turns out that this linear Eulerian upwind-biased scheme is the same as Colella's second-order corner transport upwind algorithm (Colella 1990) when no monotonicity constraint (limiter) is enforced. To aid in comparison with its semi-Lagrangian counterpart to be presented later, we provide here the complex amplification factor A resulting from the von Neumann stability analysis as a function of the nondimensionalized east–west (k) and north–south (l) wavenumbers:

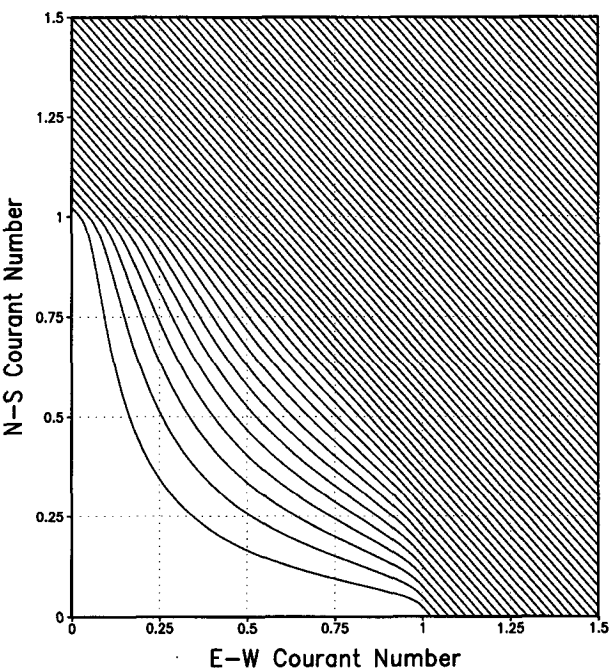

FIG. A4. The maximum amplification factor of the linear van Leer scheme in 2D without cross terms. Contour interval is 0.05. The first contour is 1.05.

$$A = 1 - C^x(1 - e^{-ik})\left[1 - \frac{1}{4}(1 - C^x)(1 - e^{-2ik})\right] \times \left[1 - \frac{1}{2}C^y(1 - e^{-il})\right] - C^y(1 - e^{-il}) \times \left[1 - \frac{1}{4}(1 - C^y)(1 - e^{-2il})\right] \times \left[1 - \frac{1}{2}C^x(1 - e^{-ik})\right], \quad \text{(A.6)}$$

where $i = \sqrt{-1}$. The directional symmetry of (A.6) is clear. The maximum and minimum magnitudes of A are solved numerically and are plotted in Figs. A1 and A2, respectively. The scheme is stable in the region described by (2.4). The minimum amplification factor provides a measure of the numerical diffusion of the particular scheme. The scheme is most damped when $C^x = C^y = 0.5$. It is informative to study the stabilizing effect of the cross terms and the effect of an asymmetric cross term as it appears in scheme (2.16) or (2.20). The amplification factor for scheme (2.24) without the cross terms (i.e., without the contribution from the inner advective operators) is

$$A^* = 1 - C^x(1 - e^{-ik}) \times \left[1 - \frac{1}{4}(1 - C^x)(1 - e^{-2ik})\right] - C^y(1 - e^{-il}) \times \left[1 - \frac{1}{4}(1 - C^y)(1 - e^{-2il})\right], \quad \text{(A.7)}$$

and the amplification factor for the asymmetric scheme (2.16) is

$$A^{**} = 1 - C^x(1 - e^{-ik}) \times \left[1 - \frac{1}{4}(1 - C^x)(1 - e^{-2ik})\right] - C^y(1 - e^{-il})\left[1 - \frac{1}{4}(1 - C^y)(1 - e^{-2il})\right] \times [1 - C^x(1 - e^{-ik})]. \quad \text{(A.8)}$$

It is found that the stable region of the asymmetric scheme (2.16) or (2.20) is the same as the symmetric scheme (2.24), as expected. But the amplification/damping factor as given by (A.8) is not symmetric to the line $C^x = C^y$. Directional biases can therefore appear in a numerical simulation. Figure A3 shows the differences of the minimum amplification factor between the symmetric and the asymmetric schemes. Overall, the asymmetric scheme appears to be more damped (diffusive) than the recommended symmetric scheme.

The maximum amplification factor of the scheme without the cross terms is plotted in Fig. A4. Although the amplification rate is very close to one in the region where $C^x + C^y \leq 1$, it is greater than one in the entire domain

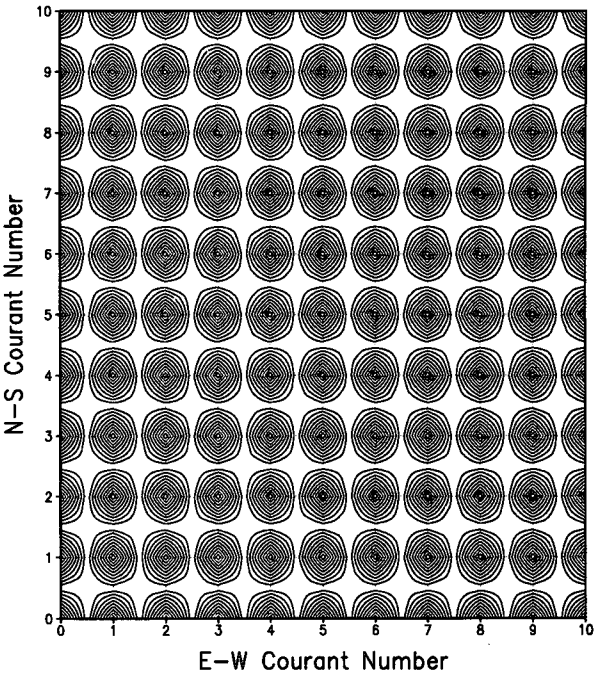

FIG. A5. The minimum amplification factor of the 2D flux-form semi-Lagrangian scheme (with linear second-order van Leer scheme as 1D outer operators for computing the fractional fluxes). Contour interval is 0.1. The first contour is 0.1. The amplification factor is exactly one for integer Courant numbers.

except in the degenerate case: $C^x = 0$ or $C^y = 0$. The scheme is, therefore, formally unstable. In 2D, the stability characteristics of the "linear" van Leer scheme without the cross terms appears to be very similar to that of the Lax–Wendroff (see Leith 1965). It should be noted that the donor-cell scheme is stable [in the region described by (2.5)] without the cross terms, as can be easily proved by dropping the second-order terms in the above analysis. The unidirectional second- (or higher) order terms are thus responsible for the destabilization. The *monotonic* (nonlinear) van Leer scheme locally reduces to the donor-cell scheme when overshoots/undershoots are to appear. Therefore, it is possible that the nonlinear van Leer scheme will be stable without the cross terms. Unfortunately, the von Neumann stability analysis is not applicable when monotonicity constraint is enforced. We have tested the 3D global (hydrostatic) chemistry transport model (described in section 4c) with the cross terms omitted in all three directions and found that a stable integration can be maintained by halving the size of the time step, but the results appear to be more diffusive without the cross terms. One possible explanation is that in regions where unrealistic amplification of the field due to linear instability (induced by the unidirectional higher order terms) is about to appear the field becomes locally unsmooth and consequently the second-order nonlinear scheme locally reduces to the first-order but stable donor-cell scheme due to the presence of the monotonicity constraint.

APPENDIX B

Stability of the 2D Flux-Form Semi-Lagrangian Scheme

The stability of the 2D semi-Lagrangian extension of the multidimensional flux-form scheme (3.9) can be similarly analyzed. To enable the von Neumann analysis, the Courant numbers in the x and y directions are again assumed to be positive definite constants and no monotonicity constraint shall be applied to the flux-form van Leer operators [see Eq. (3.13)]. Under these assumptions, the complex amplification factor A for scheme (3.9) is

$$A = 1 - \left\{1 - e^{-iMk} + c_x e^{-iMk}(1 - e^{-ik})\left[1 - \frac{1}{4}(1 - c_x)(1 - e^{-2ik})\right]\right\}\frac{1}{2}\{1 + e^{-iNl}[1 - c_y(1 - e^{-il})]\}$$

$$- \left\{1 - e^{-iNl} + c_y e^{-iNl}(1 - e^{-il})\left[1 - \frac{1}{4}(1 - c_y)(1 - e^{-2il})\right]\right\}\frac{1}{2}\{1 + e^{-iMk}[1 - c_x(1 - e^{-ik})]\}, \quad \text{(B.1)}$$

where $i = \sqrt{-1}$, $C^x = \Delta tU/\Delta x$, $M = \text{INT}(C^x)$, $c_x = C^x - M$, the fractional Courant number in the x direction, $C^y = \Delta tV/\Delta y$, $N = \text{INT}(C^y)$, and $c_y = C^y - N$, the fractional Courant number in the y direction.

Note that (B.1) reduces to the Eulerian case (A.6) when $M = N = 0$. It is found that the magnitude of A is no greater than unity for all wavenumbers (between 0 and 2π) and for all Courant numbers searched numerically (between 0 and 10). The scheme is hereby regarded as unconditionally stable for the nondeformational flow case analyzed here. In a more general deformational flow field, the stability should be limited by (3.6). Figure A5 shows the minimum value of $|A|$ (the damping factor). Although we were not able to show it analytically, the damping factor seems to be only a function of the two fractional Courant numbers. This behavior is meaningful because the shift operation that defines the integer translation is exact, and the stability characteristics of the fractional flux should be valid between each integer interval. This is exhibited by the morphology of Fig. A5.

APPENDIX C

Alternative Constraints for PPM

The two alternative constraints proposed in section 4 as well as a simplified monotonicity constraint for PPM will be described here. We will use similar notations as in Colella and Woodward (1984, CW hereafter). The simplified monotonicity constraint requires fewer floating point operations, but it is otherwise functionally equivalent to that of CW [their Eq. (1.10)]. Denoting A, a_L, a_R, and a_6 as the mean value, left edge value, right edge value, and the "curvature" of the first-guess parabola [computed by (1.5) and (1.6) in CW], over- and undershoots can be eliminated by the following Fortran-like procedure:

```
IF  ΔA_mono = 0  THEN
    A_L ← A,  A_R ← A,  A_6 ← 0
ELSE IF  a_6δa < −(δa)²  THEN
    A_6 ← 3(a_L − A),  A_R ← a_L − A_6,  A_L ← a_L
ELSE IF  a_6δa > (δa)²  THEN
    A_6 ← 3(a_R − A),  A_L ← a_R − A_6,  A_R ← a_R
ENDIF,
```

where $\delta a = a_R - a_L$, ΔA_{mono} the monotonized "slope" [determined by Eq. (1.8) in CW or Eq. (5) in L94], and A_L, A_R, and A_6 are the final left edge value, right edge value, and the curvature, respectively, of the monotonized parabola.

If only undershoots are to be eliminated, the "semi-monotonic" constraint is enforced by the following procedure:

```
IF  |δa| < −a_6  THEN
  IF  A < MIN(a_R, a_L)  THEN
      A_L ← A,  A_R ← A,  A_6 ← 0
  ELSE
      IF a_R > a_L  THEN
      A_6 ← 3(a_L − A),  A_R ← a_L − A_6,  A_L ← a_L
      ELSE
      A_6 ← 3(a_R − A),  A_L ← a_R − A_6,  A_R ← a_R
      ENDIF
  ENDIF
ENDIF.
```

If only negative undershoots are to be eliminated, the "positive definite" constraint is enforced by the following procedure:

IF $|\delta a| < -a_6$ THEN
  IF $A_{\min} < 0$ THEN
    IF $A < \text{MIN}(a_R, a_L)$ THEN
      $A_L \leftarrow A, \quad A_R \leftarrow A, \quad A_6 \leftarrow 0$
    ELSE
      IF $a_R > a_L$ THEN
      $A_6 \leftarrow 3(a_L - A), \quad A_R \leftarrow a_L - A_6,$
      $A_L \leftarrow a_L$
      ELSE
      $A_6 \leftarrow 3(a_R - A), \quad A_L \leftarrow a_R - A_6,$
      $A_R \leftarrow a_R$
      ENDIF
    ENDIF
  ENDIF
ENDIF,

where $A_{\min} = A + (a_6/12)[1 + 3(\delta a/a_6)^2]$ the minimum value of the first-guess parabolic distribution.

REFERENCES

Allen, D. J., A. R. Douglass, R. B. Rood, and P. D. Guthrie, 1991: Application of a monotonic upstream-biased transport scheme to three-dimensional constituent transport calculations. *Mon. Wea. Rev.*, **119,** 2456–2464.

Bates, J. R., and A. McDonald, 1982: Multiply-upstream, semi-Lagrangian advection schemes: Analysis and application to a multilevel primitive equations model. *Mon. Wea. Rev.*, **110,** 1831–1842.

Bell, J. B., C. N. Dawson, and G. R. Shubin, 1988: An unsplit, higher order Godunov method for scalar conservation laws in multidimensions. *J. Comput. Phys.*, **74,** 1–24.

Boris, J. P., and D. L. Book, 1973: Flux corrected transport I, SHASTA, a fluid transport algorithm that works. *J. Comput. Phys.*, **11,** 38–69.

Bott, A., 1993: The monotone area-preserving flux-form advection algorithm: Reducing the time-splitting error in the two-dimensional flow fields. *Mon. Wea. Rev.*, **121,** 2638–2641.

Brenier, Y., 1984: Averaged multivalued solutions for scalar conservation laws. *SIAM J. Num. Anal.*, **21,** 1013–1037.

Carpenter, R. L., Jr., K. K. Drogemeier, P. R. Woodward, and C. E. Hane, 1990: Application of the piecewise parabolic method to meteorological modeling. *Mon. Wea. Rev.*, **118,** 586–612.

Cohn, S. E., 1993: Dynamics of short-term univariate forecast error covariances. *Mon. Wea. Rev.*, **121,** 3123–3149.

Colella, P., 1990: Multidimensional upwind methods for hyperbolic conservation laws. *J. Comput. Phys.*, **87,** 171–200.

——, and P. R. Woodward, 1984: The piecewise parabolic method (PPM) for gas-dynamical simulations. *J. Comput. Phys.*, **54,** 174–201.

——, and H. M. Glaz, 1985: Efficient solution algorithms for the Riemann problem for real gases. *J. Comput. Phys.*, **59,** 264–289.

Douglass, A., and Coauthors, 1993: A 3 dimensional simulation of the early winter disturbution of reactive chlorine in the north polar vortex. *Geophys. Res. Lett.*, **20,** 1271–1274.

——, C. J. Weaver, R. B. Rood, and L. Coy, 1996: A three dimensional simulation of the ozone annual cycle using winds from a data assimilation system. *J. Geophys. Res.*, **101,** 1463–1474.

Dukowicz, J. K., and J. D. Ramshaw, 1979: Tensor viscosity method for convection in numerical fluid dynamics. *J. Comput. Phys.*, **32,** 71–79.

Ekebjærg, L., and P. Justesen, 1991: An explicit scheme for advection-diffusion modelling in two dimensions. *Comput. Methods Appl. Mech. Eng.*, **88,** 287–297.

Fahey, D. W., S. Solomon, S. R. Kawa, M. Loewenstein, J. R. Podolske, S. E. Strahan, and K. R. Chan, 1990: A diagnostic for denitrification in the winter polar stratospheres. *Nature,* **345,** 698–702.

Haltiner, G. J., and R. T. Williams, 1980: *Numerical Prediction and Dynamic Meteorology,* Wiley and Sons, 477 pp.

Laprise, J. P. R., and A. Plante, 1995: A class of semi-Lagrangian integrated-mass numerical transport algorithms. *Mon. Wea. Rev.*, **123,** 553–565.

Leith, C. E., 1965: Numerical simulation of the earth's atmosphere. *Method in Computational Physics.* Vol. 4, Academic Press, 385 pp.

Leonard, B. P., 1994: Note on the von Neumann stability of explicit one-dimensional advection schemes. *Comput. Methods Appl. Mech. Eng.*, **118,** 29–46.

LeVeque, R. J., 1985: A large timer step generalization of Godunov's method for systems of conservation laws. *SIAM J. Num. Anal.*, **22,** 1051–1073.

——, 1993: High-resolution conservative algorithms for advection in incompressible flow. Tech. Rep. 93-03, University of Washington, Seattle, WA, 40 pp.

Lin, S.-J., W. C. Chao, Y. C. Sud, and G. K. Walker, 1994: A class of the van Leer–type transport schemes and its applications to the moisture transport in a general circulation model. *Mon. Wea. Rev.*, **122,** 1575–1593.

McRae, G. J., W. R. Goodin, and J. H. Seinfeld, 1982: Numerical solution of the atmospheric diffusion equation for chemically reacting flows. *J. Comput. Phys.*, **45,** 1–42.

Mesinger, F., and A. Arakawa, 1976: Numerical methods used in atmospheric models. GARP Publications Series 17, WMO-ICSU Joint Organizing Committee, 64 pp.

Petschek, A. G., and L. D. Libersky, 1975: Stability, accuracy, and improvement of the Crowley advection schemes. *Mon. Wea. Rev.*, **103,** 1104–1109.

Plumb, R. A., and M. K. W. Ko, 1992: Interrelationships between mixing ratios of long-lived stratospheric constituents. *J. Geophys. Res.*, **97,** 10 145–10 156.

Prather, M. J., 1986: Numerical advection by conservation of second-order moments. *J. Geophys. Res.*, **91,** 6671–6681.

Priestley, A., 1993: A quasi-conservative version of the semi-Lagrangian advection scheme. *Mon. Wea. Rev.*, **121,** 621–629.

Rancic, M., 1992: Semi-Lagrangian piecewise biparabolic scheme for two-dimensional horizontal advection of a passive scalar. *Mon. Wea. Rev.*, **120,** 1394–1406.

Rasch, P. J., 1994: Conservative shape-preserving two-dimensional transport on a spherical reduced grid. *Mon. Wea. Rev.*, **122,** 1337–1350.

Ritchie, H., 1986: Eliminating the interpolation associated with the semi-Lagrangian scheme. *Mon. Wea. Rev.*, **114,** 135–146.

Roache, P. J., 1992: A flux-based modified method of characteristics. *Int. J. Numer. Methods Fluids,* **15,** 1259–1275.

Rood, R., 1987: Numerical advection algorithms and their role in atmospheric transport and chemistry models. *Rev. Geophys.*, **25,** 71–100.

——, D. Allen, W. Baker, D. Lamich, and J. Kaye, 1989: The use of assimilated stratospheric data in constituent transport calculations. *J. Atmos. Sci.*, **46,** 687–701.

——, and Coauthors, 1991: Three-dimensional simulations of wintertime ozone variability in the lower stratosphere. *J. Geophys. Res.*, **96,** 5055–5071.

——, A. R. Douglass, J. A. Kaye, and D. B. Considine, 1993: Characteristics of wintertime and autumn nitric acid chemistry as defined by LIMB infrared monitor of the stratosphere (LIMS) data. *J. Geophys. Res.*, **98,** 18 533–18 545.

Schneider, H. R., 1984: A numerical transport scheme that avoids negative mixing ratios. *Mon. Wea. Rev.*, **112,** 1206–1217.

Schubert, S. D., R. B. Rood, and J. Pfaendtner, 1993: An assimilated dataset for earth science applications. *Bull. Amer. Meteor. Soc.*, **74,** 2331–2342.

Smolarkiewicz, P. K., 1982: The multi-dimensional Crowley advection scheme. *Mon. Wea. Rev.*, **110,** 1968–1983.

——, 1983: A simple positive definite advection scheme with small implicit diffusion. *Mon. Wea. Rev.*, **111,** 479–486.

——, 1984: A fully multidimensional positive definite advection transport algorithm with small implicit diffusion. *J. Comput. Phys.*, **54,** 325–362.

——, and W. W. Grabowski, 1990: The multidimensional positive definite advection transport algorithm: Nonoscillatory option. *J. Comput. Phys.*, **86,** 335–375.

——, and P. J. Rasch, 1991: Monotone advection on the sphere: An Eulerian versus semi-Lagrangian approach. *J. Atmos. Sci.*, **48,** 793–810.

——, and G. A. Grell, 1992: A class of monotone interpolation schemes. *J. Comput. Phys.*, **101,** 431–440.

——, and J. A. Pudykiewicz, 1992: A class of semi-Lagrangian approximation for fluids. *J. Atmos. Sci.*, **49,** 2082–2096.

Staniforth, A., and J. Côté, 1991: Semi-Lagrangian integration schemes for atmospheric models—A review. *Mon. Wea. Rev.*, **119,** 2206–2223.

Strang, G., 1968: On the construction and comparison of difference schemes. *SIAM J. Num. Anal.*, **5,** 506–517.

Takacs, L. L., A. Molod, and T. Wang, 1994: Documentation of the Goddard earth observing system general circulation model—Version 1. NASA Tech. Memo 104606, 100 pp.

van Leer, B., 1974: Toward the ultimate conservative difference scheme. Part II: Monotonicity and conservation combined in a second order scheme. *J. Comput. Phys.*, **14,** 361–370.

——, 1977: Toward the ultimate conservative difference scheme. Part IV: A new approach to numerical convection. *J. Comput. Phys.*, **23,** 276–299.

——, 1979: Toward the ultimate conservative difference scheme. Part V: A second order sequel to Godunov's method. *J. Comput. Phys.*, **32,** 101–136.

Williamson, D. L., and P. J. Rasch, 1989: Two-dimensional semi-Lagrangian transport with shape preserving interpolation. *Mon. Wea. Rev.*, **117,** 102–129.

——, J. B. Drake, J. J. Hack, R. Jakob, and P. N. Swarztrauber, 1992: A standard test set for numerical approximations to the shallow water equations in spherical geometry. *J. Comput. Phys.*, **102,** 211–224.

Woodward, P. R., and P. Colella, 1984: The numerical simulation of two-dimensional fluid flow with strong shocks. *J. Comput. Phys.*, **54,** 115–173.

Zalesak, S. T., 1979: Fully multidimensional flux-corrected transport algorithms for fluid. *J. Comput. Phys.*, **31,** 335–362.